Chaire de Physique
de la Matière Condensée
Antoine Georges

De l'effet Hall quantique aux matériaux moirés

- Topologie et géométrie des matériaux quantiques -

Cours 6 – Matériaux moirés: pourquoi des bandes plates?

Modèle continu (Bistritzer-MacDonald), limite chirale.

Quelques effets des interactions

Cycle 2025-2026
3 juin 2026

Chaire de Physique
de la Matière Condensée
Antoine Georges

From the Quantum Hall Effect to Moiré Materials
- Topology and Geometry of Quantum Materials -

Lecture 6 – Moiré materials: why flat bands?

Continuous model of TBLG (Bistritzer-MacDonald), chiral limit.

Some effects of strong correlations

2025-2026 Lectures
June 3, 2026

Antoine GEORGES

CHAIRE PHYSIQUE DE LA MATIÈRE CONDENSÉE

De l'effet Hall quantique aux matériaux moirés : topologie et géométrie des matériaux quantiques

6 mai > 3 juin 2026

COLLÈGE DE FRANCE 1530

Thomas Römer
Administrateur du Collège de France
11, place Marcelin-Berthelot, 75005 Paris
www.college-de-france.fr

Année académique 2025/2026

Mercredi 3 juin 2026

Amphithéâtre Guillaume Budé

9h30 : Cours – Antoine Georges

Matériaux moirés: pourquoi des bandes plates? Modèle continu (Bistritzer-MacDonald), limite chirale. Quelques effets des interactions.

11h30 : Séminaire – Gwendal Fève

(Ecole Normale Supérieure)

Electron optics experiments in quantum Hall conductors: from single electrons to anyons

Abstract: In the quantum Hall regime, the ballistic propagation of electronic waves, combined with electrostatic gates for current partitioning, enables the realization of electronic interferometers. I will discuss how these electron optics experiments can be extended to the fractional quantum Hall regime to probe its elementary excitations called anyons, revealing their fractional charge and fractional statistics.

Les cours seront enregistrés et diffusés sur le site web de la chaire après la date de la séance. Inscription sur la liste de diffusion : envoyer un message à listes-diffusion.cdf@college-de-france.fr avec comme sujet : subscribe chaire-pmc.ipcdf

Acknowledgements

I am grateful to the many colleagues who helped me understand (somewhat) TBLG and especially to:

Lorenzo Crippa

Giorgio Sangiovanni

Andrei Bernevig

Nicolas Regnault

Valentin Crépel

And to all co-authors of this paper:

PHYSICAL REVIEW X **14,** 031045 (2024)

Dynamical Correlations and Order in Magic-Angle Twisted Bilayer Graphene

Gautam Rai,[1,*] Lorenzo Crippa,[2,*] Dumitru Călugăru,[3] Haoyu Hu,[4] Francesca Paoletti,[2] Luca de' Medici,[5] Antoine Georges,[6,7,8,9] B. Andrei Bernevig,[3,4,10] Roser Valentí,[11] Giorgio Sangiovanni,[2,†] and Tim Wehling[1,12,‡]

Twisted Graphene

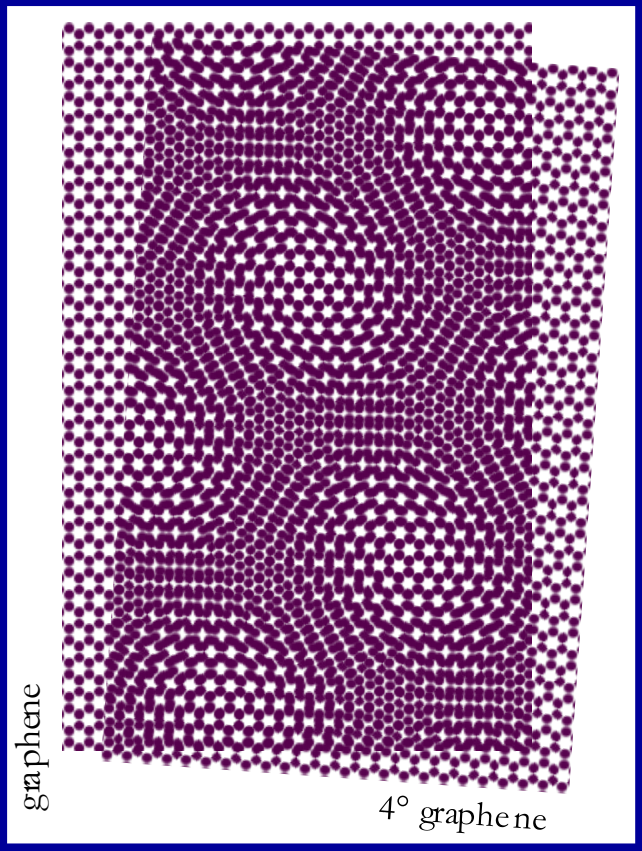

Credit:Wikipedia

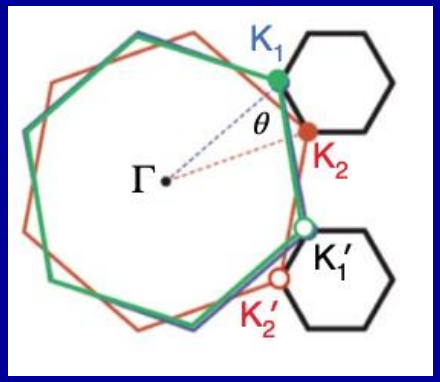

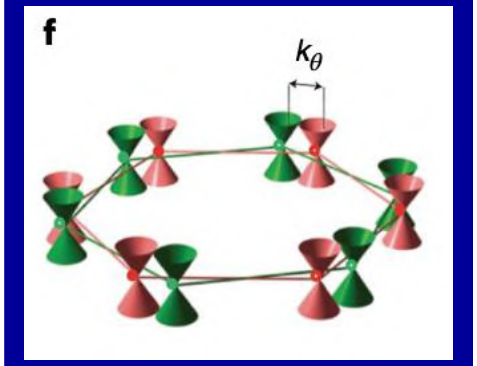

Credit:
E.Andrei
A.MacDonald
Nature Mat

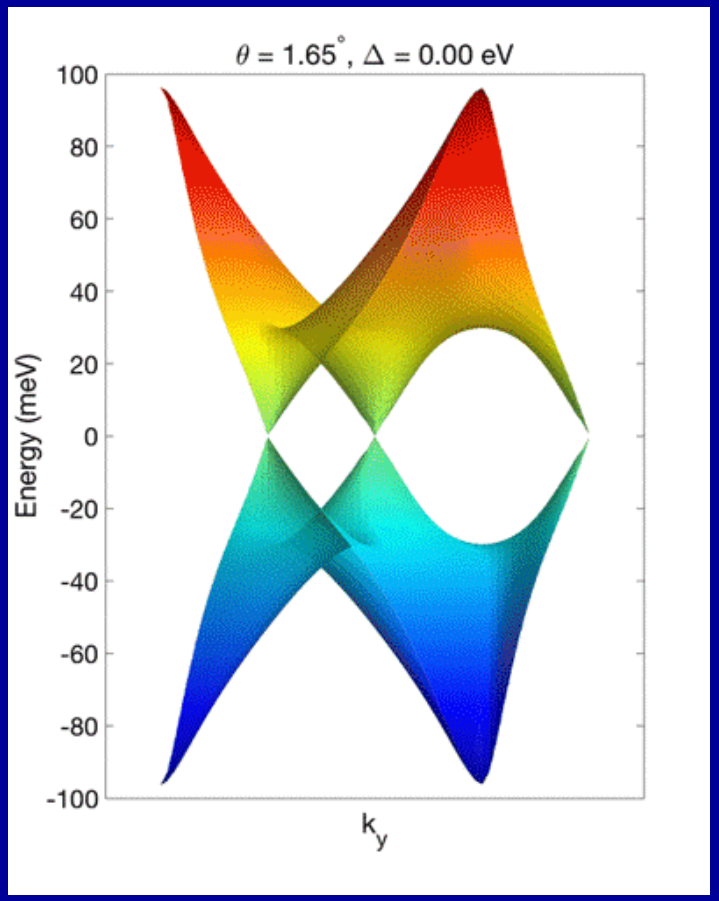

Credit: B. Chittari/University of Seoul

Moire [from Wikipedia]

Pour les articles homonymes, voir Moire (homonymie).

La **moire** est un tissu disposant d'un effet d'ondulation obtenu par calandrage lors de sa fabrication. Elle désigne aussi par extension l'effet visuel analogue à celui provoqué par ce textile (éclat changeant, apparence ondée et chatoyante).

Historique [modifier | modifier le code]

Robe moirée, détail du tableau de Francesco Hayez, *Portrait de la princesse de Sant' Antimo*, conservé au Musée National de San Martino, Naples

Le mot existe en anglais dès le XVII^e siècle sous la graphie de mohair, empruntée de l'arabe. Il ne désigne alors pas spécifiquement un tissu moiré. En 1669, le règlement de Colbert détaille ce qui peut être nommé moire, alors composé de soie pure cuite ou crue, avec quatre largeurs autorisées, et une lisière de couleur différente. Il n'y a pas de mention de l'effet moiré. Le terme connait de nombreuses variantes.

Au XVIII^e siècle, la moire désigne une sorte de Gros de Tours, parfois façonné, et doté d'effet d'ombres par écrasement[a 1].

Définition moderne [modifier | modifier le code]

De nos jours, la moire désigne de manière figée le tissu obtenu par le procédé de Tignat inventé en 1843, fabricant lyonnais, qui consiste à écraser par calandrage sous tension un tissu en le repliant sur lui-même (tête contre tête). La trame dévie alors légèrement et acquiert un effet ondulé par réflexion de la lumière. Le décor sinueux est déterminé par le type de pliage utilisé, qui place des reflets en forme de cercles concentriques[a 2]. Il en existe une grande quantité de variantes[a 3].

Ruban moiré

Utilisations [modifier | modifier le code]

TBLG: A Cornucopia of Phases!

Cao et al.
Nature 556, 43 (2018)
Discovery of SC
at magic angle:

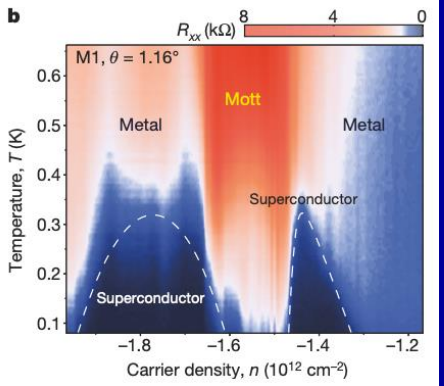

LMU LUDWIG-MAXIMILIANS-UNIVERSITÄT MÜNCHEN

Most reproducible MATBG phase diagram

Open questions?

Efetov Lab

From D.Efetov's seminar on May 13

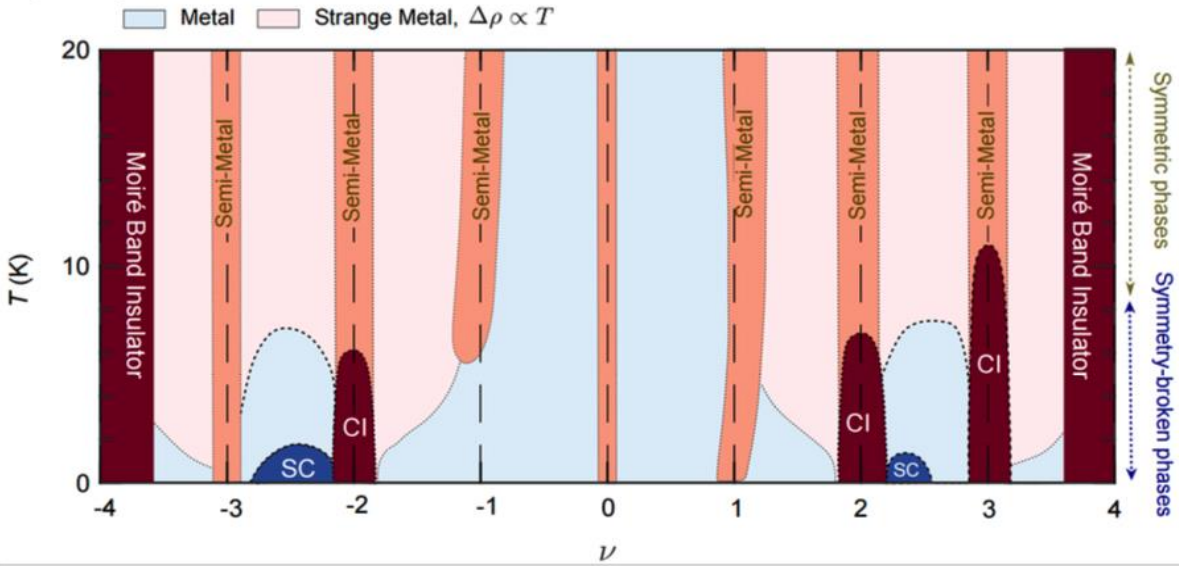

States at integer filling $\nu = 0, \pm1, \pm2, \pm3$:

- T > 10K → all show semi-metallic resistance peaks.
- T < 10K → distinct behaviour of $\nu = -1, -2$ etc. Clear signatures of symmetry breaking set-in (Hall resets).

Superconductivity:

- By far most common and strongest for $\nu = -2 - \delta$ and less common for $\nu = 2 + \delta$. All other regions rare.

Metallic states:

- T > 10K → broad range of R ~ T strange metal.
- T < 10K → many region become good metals.
- New → between $\nu = \pm2 - \pm3$, a previously overlooked metallic dome, which can be associated with the pseudo-gap and IVC order. SC originates predominantly in this metallic state.

More broadly:
moiré two-dimensional materials

TMDs:van der Waals layered materials

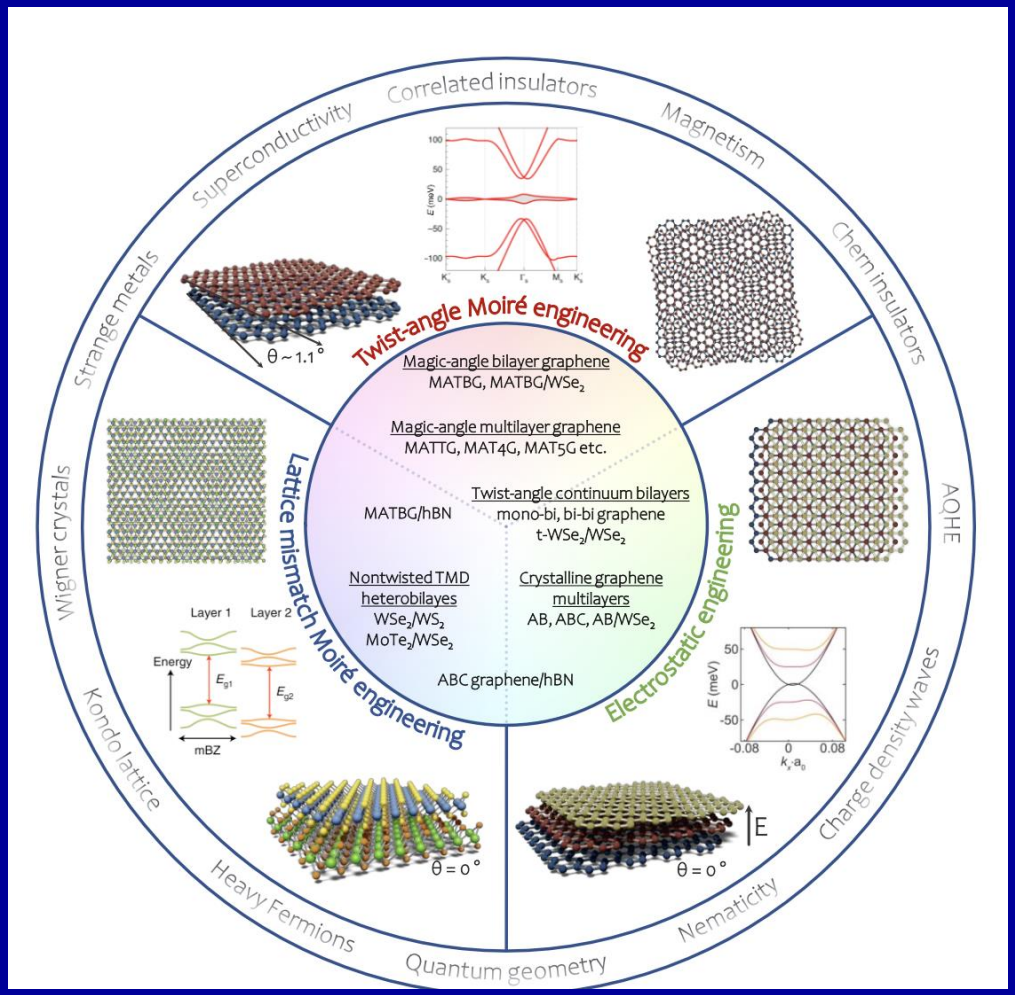

From D.Efetov's seminar

nature physics

REVIEW ARTICLE

https://doi.org/10.1038/s41567-020-01154-3

Check for updates

Moiré heterostructures as a condensed-matter quantum simulator

Dante M. Kennes[1,2,12]✉, Martin Claassen[3,4,12], Lede Xian[2,5,12], Antoine Georges[3,6,7,8], Andrew J. Millis[3,9], James Hone[10], Cory R. Dean[9], D. N. Basov[9], Abhay N. Pasupathy[9]✉ and Angel Rubio[2,3,11]✉

Thousands of candidates 'twistable' materials:

arXiv:2411.09741

2D Theoretically Twistable Material Database

Yi Jiang,[1,*] Urko Petralanda,[2,*] Grigorii Skorupskii,[3,*] Qiaoling Xu,[4,5] Hanqi Pi,[1] Dumitru Călugăru,[6] Haoyu Hu,[1,7] Jiaze Xie,[3] Rose Albu Mustaf,[8,9,10] Peter Höhn,[11] Vicky Haase,[11] Maia G. Vergniory,[12,1] Martin Claassen,[13] Luis Elcoro,[2] Nicolas Regnault,[14,6,15] Jie Shan,[16,17,18] Kin Fai Mak,[16,17,18] Dmitri K. Efetov,[19,20] Emilia Morosan,[8,9,10] Dante M. Kennes,[21,22] Angel Rubio,[22,14,23] Lede Xian,[5,24,22] Claudia Felser,[11] Leslie M. Schoop,[3] and B. Andrei Bernevig[6,1,25,†]

arXiv:2512.15851

High-throughput discovery of moiré homobilayers guided by topology and energetics

Naoto Nakatsuji,[1] Jennifer Cano,[1,2] and Valentin Crépel[3]

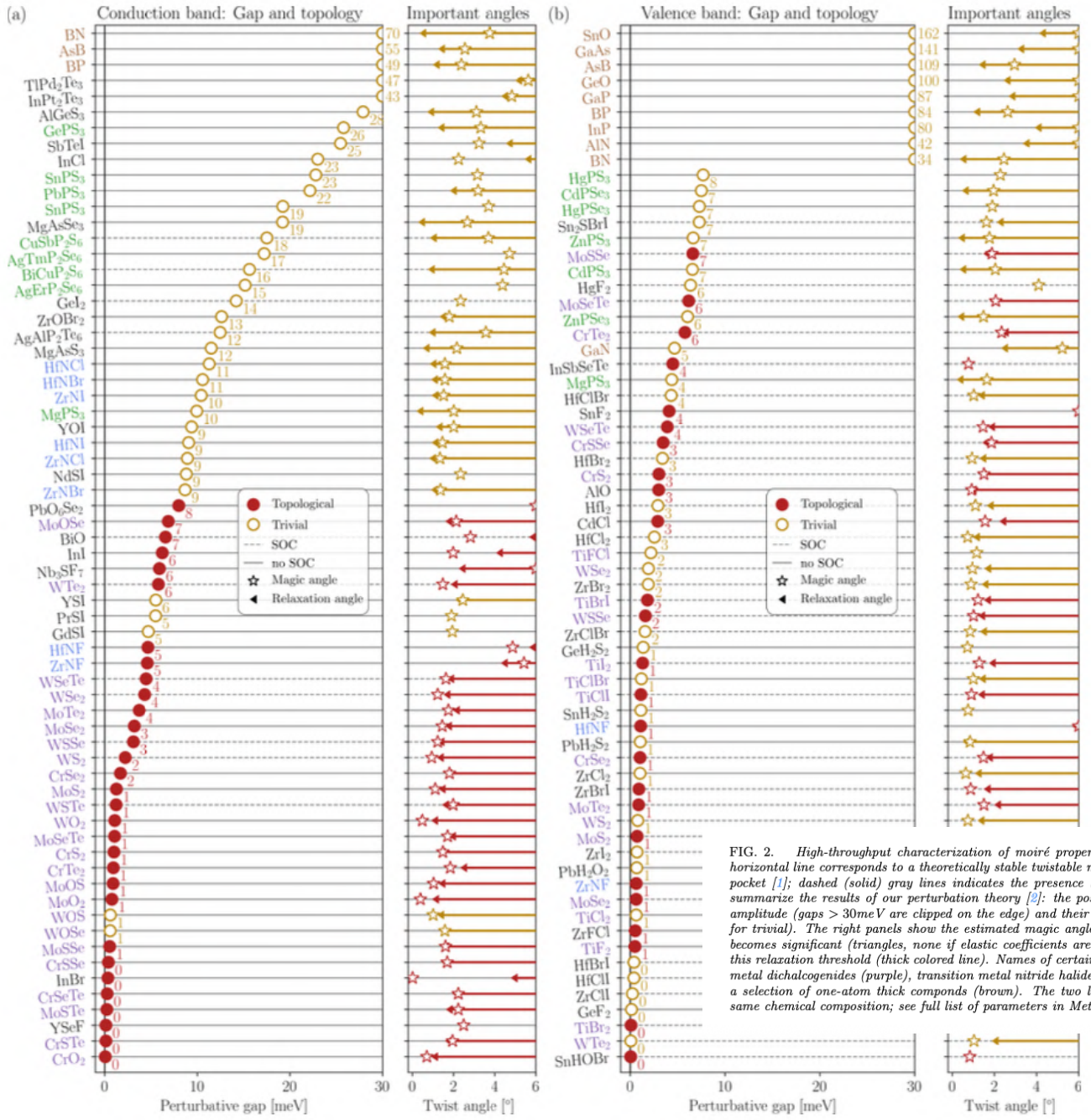

FIG. 2. *High-throughput characterization of moiré properties for all K-valley semiconducting moiré homobilayers. Each horizontal line corresponds to a theoretically stable twistable material with either (a) an electron-like or (b) a hole-like K-valley pocket [1]; dashed (solid) gray lines indicates the presence (absence) of spin-orbit coupling. The left panels of (a) and (b) summarize the results of our perturbation theory [2]: the position of the markers and the adjacent value gives the moiré gap amplitude (gaps $> 30meV$ are clipped on the edge) and their color encodes the topology of the bilayer (red for topological, gold for trivial). The right panels show the estimated magic angles (stars) and twist angles θ_{relax} where in-plane lattice relaxation becomes significant (triangles, none if elastic coefficients are not available). Our predictions are only formally justified above this relaxation threshold (thick colored line). Names of certain material families are colored for reference in the text: transition metal dichalcogenides (purple), transition metal nitride halides (blue), transition metal phosphorus trichalcogenide (green), and a selection of one-atom thick componds (brown). The two lines labeled $SnPS_3$ represent different crystal structures with the same chemical composition; see full list of parameters in Methods.*

arXiv:2512.15851

Moiré pattern

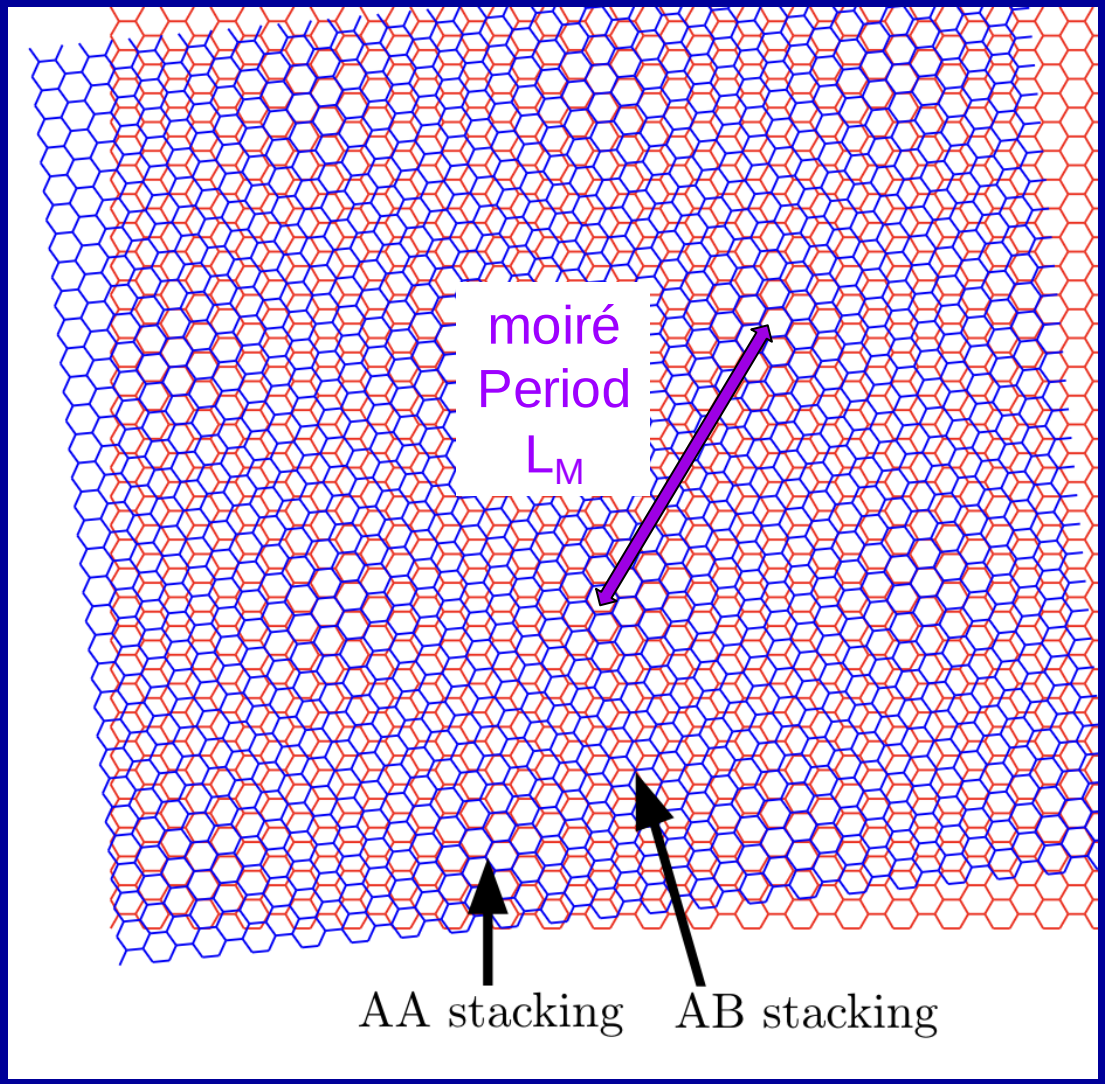

Periodic or Quasiperiodic?

PRL 99, 256802 (2007) PHYSICAL REVIEW LETTERS week ending 21 DECEMBER 2007

Graphene Bilayer with a Twist: Electronic Structure

J. M. B. Lopes dos Santos,[1] N. M. R. Peres,[2] and A. H. Castro Neto[3]

Periodic (Commensurate) for:

$$\cos\theta_n = \frac{3n^2 + 3n + 1/2}{3n^2 + 3n + 1}$$

$$n = 0, 1, 2, \cdots$$

The authors of this paper observed that the Dirac velocity is reduced at small angle and computed the first correction

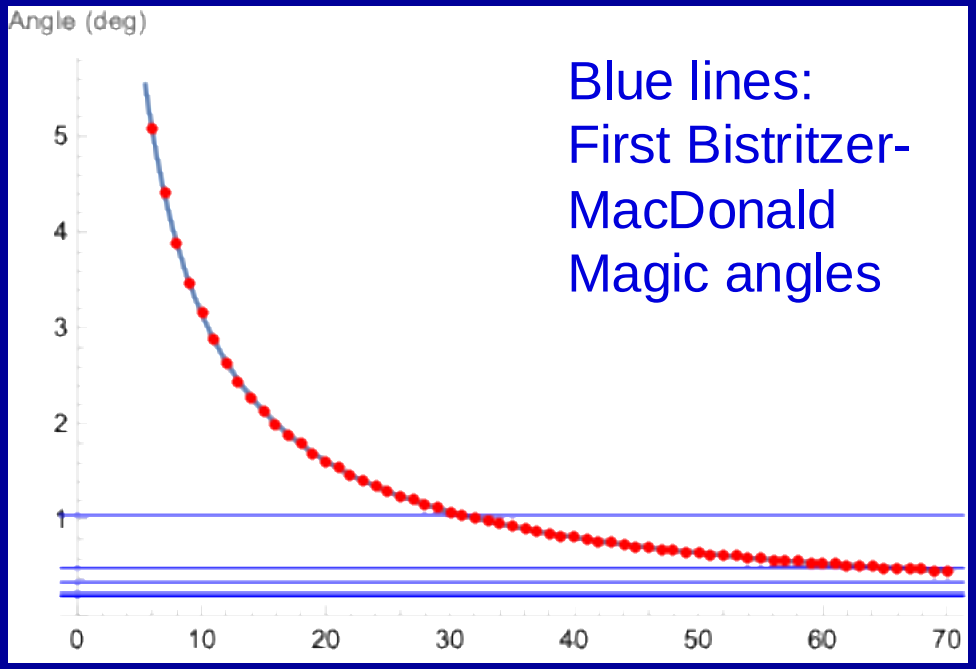

Blue lines:
First Bistritzer-MacDonald Magic angles

TBLG: Geometry

Note: In this lecture a=0.246nm is the period of the graphene Bravais lattice (not C-C bondlength)

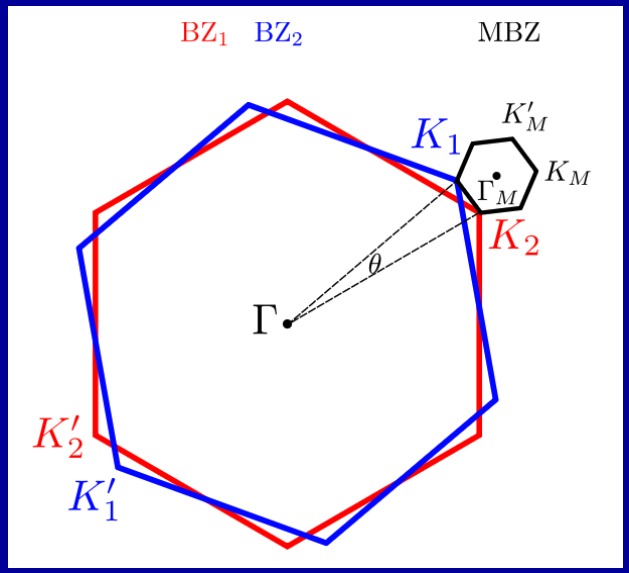

Reciprocal lattice of each layer:

$$\boldsymbol{G}_1 = \frac{4\pi}{\sqrt{3}\,a}\begin{pmatrix}\sin(\theta/2)\\ \cos(\theta/2)\end{pmatrix}, \qquad \boldsymbol{G}_2 = \frac{4\pi}{\sqrt{3}\,a}\begin{pmatrix}-\sin(\theta/2)\\ \cos(\theta/2)\end{pmatrix}$$

Smallest moiré RL vector:

$$\boldsymbol{g}_M = \boldsymbol{G}_1 - \boldsymbol{G}_2 = \frac{4\pi}{\sqrt{3}\,a}\begin{pmatrix}2\sin(\theta/2)\\ 0\end{pmatrix}$$

$$|\boldsymbol{g}_M| = \frac{8\pi\,\sin(\theta/2)}{\sqrt{3}\,a}.$$

$$|\mathbf{g}| = \frac{4\pi}{\sqrt{3}\,L_M} \Rightarrow \boxed{L_M = \frac{a}{2\sin(\theta/2)} \simeq \frac{a}{\theta}}$$

- Twist creates a **moiré superlattice** with long wavelength $L_M \gg a$
- For $\theta \sim 1°$: $L_M \sim 14\,\text{nm}$, supercell $\sim 10^4$ atoms

Why interesting?

At magic angle $\theta^* \approx 1.05°$:

$$W \lesssim 10\,\text{meV}, \quad U \sim \frac{e^2}{\epsilon L_M} \sim 20\text{–}30\,\text{meV}$$

$$\Rightarrow \quad \frac{U}{W} \gg 1 \quad \text{(strongly correlated)}$$

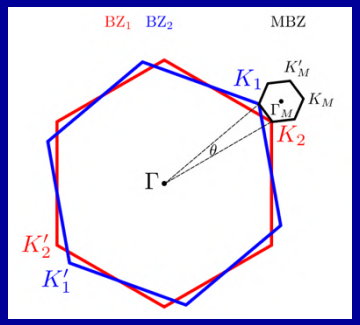

Moiré Brillouin Zone

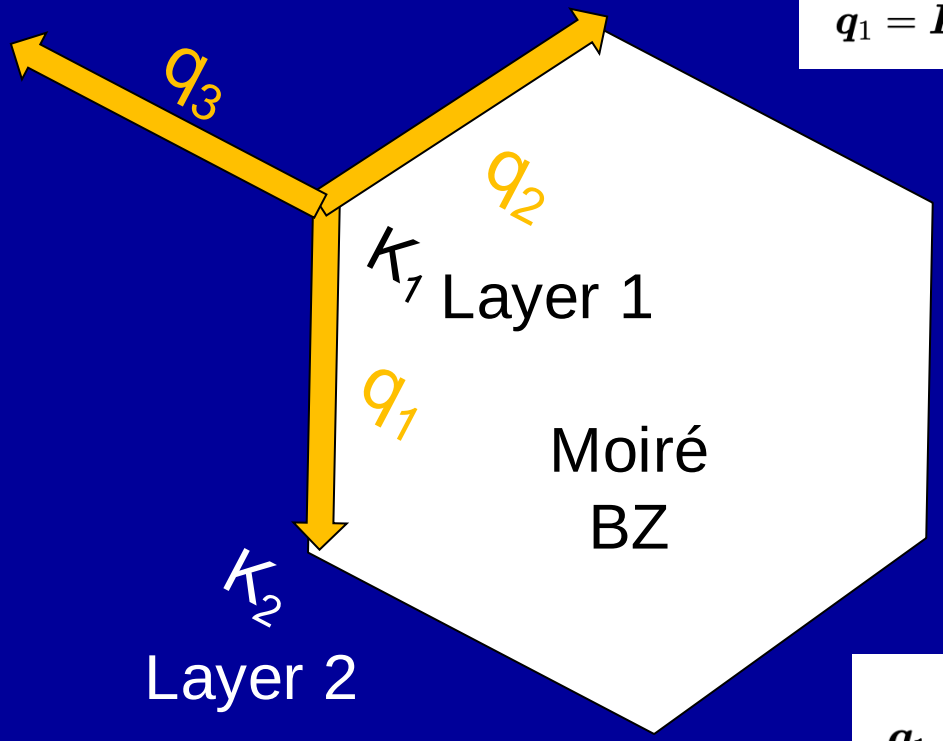

$$\boldsymbol{q}_1 = \boldsymbol{K}_2 - \boldsymbol{K}_1, \qquad \boldsymbol{q}_2 = R_{2\pi/3}\,\boldsymbol{q}_1, \qquad \boldsymbol{q}_3 = R_{4\pi/3}\,\boldsymbol{q}_1,$$

related by C_3 symmetry

$$\boldsymbol{K}_1 = R_{+\theta/2}\,\boldsymbol{K}, \qquad \boldsymbol{K}_2 = R_{-\theta/2}\,\boldsymbol{K},$$

$$|\Delta \boldsymbol{K}| = K_D\theta, \quad K_D = \frac{4\pi}{3a}.$$

$$\boldsymbol{q}_1 = K_D\theta \begin{pmatrix} 0 \\ -1 \end{pmatrix}, \qquad \boldsymbol{q}_{2,3} = K_D\theta \begin{pmatrix} \pm\sqrt{3}/2 \\ 1/2 \end{pmatrix}.$$

The moiré reciprocal lattice vectors are $\boldsymbol{g}_1 = \boldsymbol{q}_3 - \boldsymbol{q}_2$ and $\boldsymbol{g}_2 = \boldsymbol{q}_1 - \boldsymbol{q}_3$.

The Bistritzer-MacDonald Model

PNAS | **July 26, 2011** | vol. 108 | no. 30 | **12233–12237**

Moiré bands in twisted double-layer graphene

Rafi Bistritzer and Allan H. MacDonald[1]

Department of Physics, University of Texas at Austin, Austin, TX 78712

Contributed by Allan H. MacDonald, June 7, 2011 (sent for review December 8, 2010)

A moiré pattern is formed when two copies of a periodic pattern are overlaid with a relative twist. We address the electronic structure of a twisted two-layer graphene system, showing that in its continuum Dirac model the moiré pattern periodicity leads to moiré Bloch bands. The two layers become more strongly coupled and the Dirac velocity crosses zero several times as the twist angle is reduced. For a discrete set of magic angles the velocity vanishes, the lowest moiré band flattens, and the Dirac-point density-of-states and the counterflow conductivity are strongly enhanced.

WOLF FOUNDATION

Prize Share:
Allan H. MacDonald
Pablo Jarillo-Herrero
Rafi Bistritzer

Award citation:
"For pioneering theoretical and experimental work on twisted bilayer graphene."

Recall graphene:

Dirac Hamiltonian (near K)

$$H_0(\boldsymbol{k}) = \hbar v_F\, \boldsymbol{\sigma}\cdot\boldsymbol{k} = \hbar v_F \begin{pmatrix} 0 & k_x - ik_y \\ k_x + ik_y & 0 \end{pmatrix}$$

$$E_\pm = \pm\hbar v_F |\boldsymbol{k}|$$

The BM Hamiltonian:

BM Hamiltonian (single valley)

$$H_{\mathrm{BM}} = \begin{pmatrix} H_1(\boldsymbol{k}) & T(\boldsymbol{r}) \\ T^\dagger(\boldsymbol{r}) & H_2(\boldsymbol{k}) \end{pmatrix}$$

$$H_\ell(\boldsymbol{k}) = \hbar v_F R_{\mp\theta/2}\boldsymbol{k}\cdot\boldsymbol{\sigma}^{(\ell)}$$

$$\boldsymbol{\sigma}^{(1)} = (\sigma_x, \sigma_y), \quad \boldsymbol{\sigma}^{(2)} = (\sigma_x, -\sigma_y)$$

Interlayer tunneling

$$T(\boldsymbol{r}) = \sum_{j=1}^{3} T_j\, e^{i\boldsymbol{q}_j\cdot\boldsymbol{r}}$$

Three approximations (valid for $\theta \lesssim 5°$)

1. **Continuum limit**: retain only low-energy states near K-points; valid for $|\boldsymbol{k}| \ll K_D$
2. **Valley decoupling**: inter-valley scattering $\propto a/L_M \ll 1$; treat K and K' independently
3. **Three-shell tunneling**: retain only three leading moiré momentum transfers $\boldsymbol{q}_j$

Structure

- 4×4 matrix in layer $\otimes$ sublattice space
- Kinetic: Dirac cone for each layer
- Tunneling: couples layers via moiré potential $T(\boldsymbol{r})$

Acts on spinor:

$$(\psi_{A_1}, \psi_{B_1}, \psi_{A_2}, \psi_{B_2})$$

Tunneling Matrices and the BM Parameter

Tunneling matrices T_j

- $w_{AB} \approx 110\,\text{meV}$: AB tunneling amplitude
- w_{AA}: AA tunneling (suppressed by relaxation)
- Equal tunneling: $w_{AA} = w_{AB} = w$
- **Chiral limit**: $w_{AA} = 0$ (analytically tractable)
- C_3 symmetry: T_j related by 120° rotations

The BM dimensionless parameter α

- Ratio of tunneling to kinetic energy scale
- Single parameter controls all the physics
- $\alpha \approx 0.56/\theta[\text{deg}]$
- Magic angle: $\alpha^* = 1/\sqrt{3} \approx 0.577$

Tunneling matrices

$$T_j = \begin{pmatrix} w_{AA} & w_{AB} e^{-2\pi i(j-1)/3} \\ w_{AB} e^{2\pi i(j-1)/3} & w_{AA} \end{pmatrix}$$

For $w_{AA} = w_{AB} = w$: $\quad T_1 = w \begin{pmatrix} 1 & 1 \\ 1 & 1 \end{pmatrix}$

BM parameter

$$\alpha = \frac{w}{\hbar v_F K_D \theta}$$

In the BM continuous model:

- Periodicity is preserved, irrespective of whether we have a strictly periodic lattice or not!
- Periodic moiré potential → Bloch theorem applies
- Multiple hops generate a coupling between modes at a lattice of wave-vectors:

$$\mathbf{k} + n_1\mathbf{g}_1 + n_2\mathbf{g}_2 \quad (\text{layer1})$$

$$\mathbf{k} + \mathbf{q}_\mathbf{j} + n_1\mathbf{g}_1 + n_2\mathbf{g}_2 \quad (\text{layer2}, \text{j} = 1, 2, 3)$$

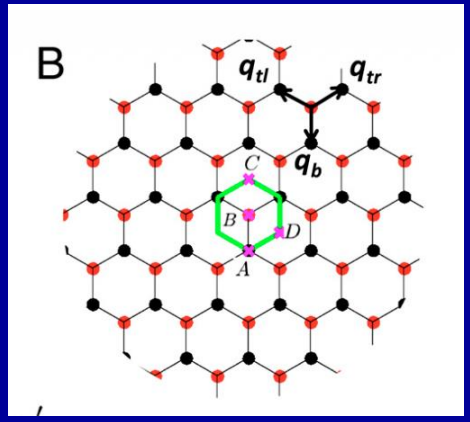

Effective Hamiltonian at k
- First shell approximation -

Consider full 8*8 Hamiltonian at k for layer 1 (and layer 2 at 3 wavevectors $k+q_j$):

$$H^{(3)}(\boldsymbol{k}) = \begin{pmatrix} \boldsymbol{\sigma}\cdot\boldsymbol{k} & T_1^\dagger & T_2^\dagger & T_3^\dagger \\ T_1 & \boldsymbol{\sigma}^{(2)}\cdot(\boldsymbol{k}+\boldsymbol{q}_1) & 0 & 0 \\ T_2 & 0 & \boldsymbol{\sigma}^{(2)}\cdot(\boldsymbol{k}+\boldsymbol{q}_2) & 0 \\ T_3 & 0 & 0 & \boldsymbol{\sigma}^{(2)}\cdot(\boldsymbol{k}+\boldsymbol{q}_3) \end{pmatrix}$$

$$H_{\text{eff}}(\boldsymbol{k}) = \boldsymbol{\sigma}\cdot\boldsymbol{k} - \sum_{j=1}^{3} T_j^\dagger \left[\boldsymbol{\sigma}^{(2)}\cdot(\boldsymbol{k}+\boldsymbol{q}_j)\right]^{-1} T_j .$$

$$\begin{bmatrix} A & B \\ C & D \end{bmatrix}^{-1} = \begin{bmatrix} (A-BD^{-1}C)^{-1} & -(A-BD^{-1}C)^{-1}BD^{-1} \\ -D^{-1}C(A-BD^{-1}C)^{-1} & D^{-1}+D^{-1}C(A-BD^{-1}C)^{-1}BD^{-1} \end{bmatrix}$$

Schur complement (elimination of lower 6*6 block)

After some algebra:

$$H_{\text{eff}}(\mathbf{k}) = \hbar v_F^* \, \sigma\cdot\mathbf{k} \ , \quad \frac{v_F^*}{v_F} = \frac{1-3\alpha^2}{1+6\alpha^2}$$

- Multiple round-trips
- Beyond perturbative

Vanishes for: $\alpha = 1/\sqrt{3} \Rightarrow \theta^* \simeq 1.05^o$ First magic angle

Magic Angles

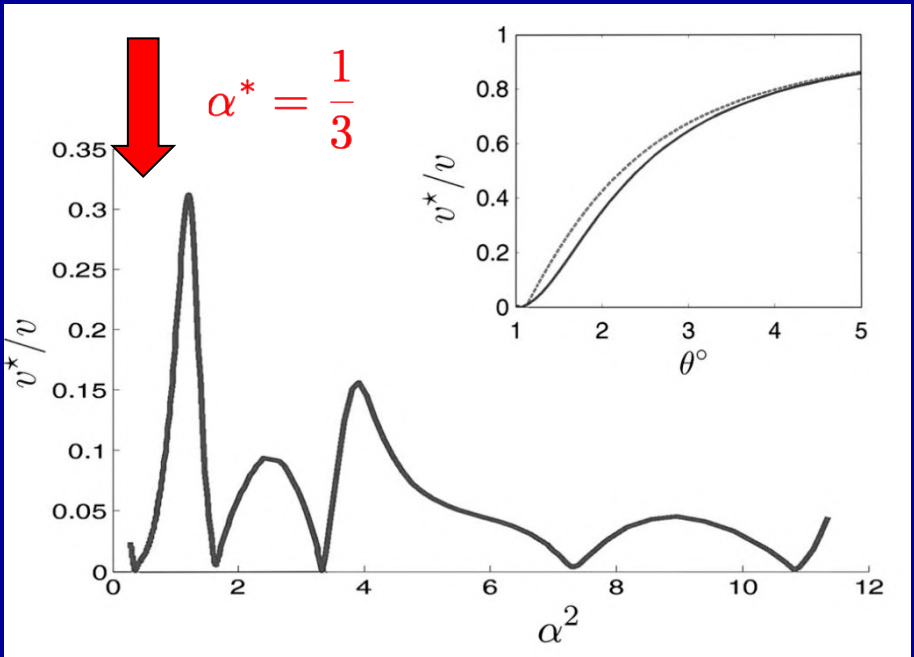

BM parameter

$$\alpha = \frac{w}{\hbar v_F K_D \theta}$$

Smaller magic angles require a full diagonalization beyond the first shell or reciprocal lattice vectors approximation

Fig. 4. Renormalized Dirac-point band velocity. The band velocity of the twisted bilayer at the Dirac point $v^\star$ is plotted vs. α^2, where $\alpha = w/vk_\theta$ for $0.18° < \theta < 1.2°$. The velocity vanishes for $\theta \approx 1.05°$, $0.5°$, $0.35°$, $0.24°$, and $0.2°$. (*Inset*) The renormalized velocity at larger twist angles. The solid line corresponds to numerical results and dashed line corresponds to analytic results based on the eight-band model.

PNAS | **July 26, 2011** | vol. 108 | no. 30 | **12233–12237**

Bands at the magic angle

Animation from Cao et al.
Nature 556, 43 (2018)

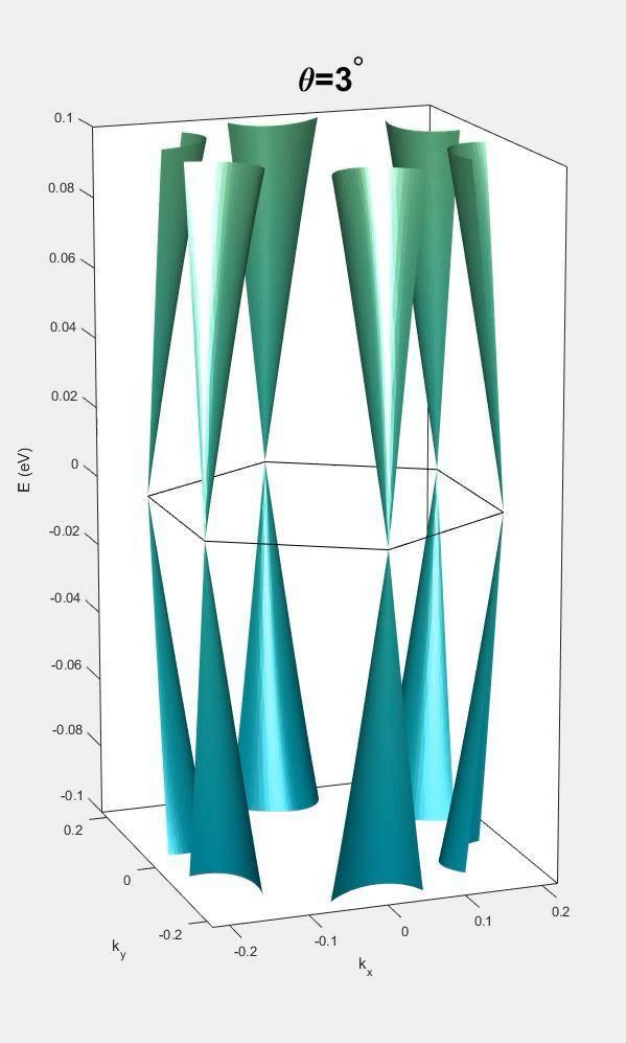

Bands at the magic angle

Fig. from Song and Bernevig
PRL 129, 047601 (2022)

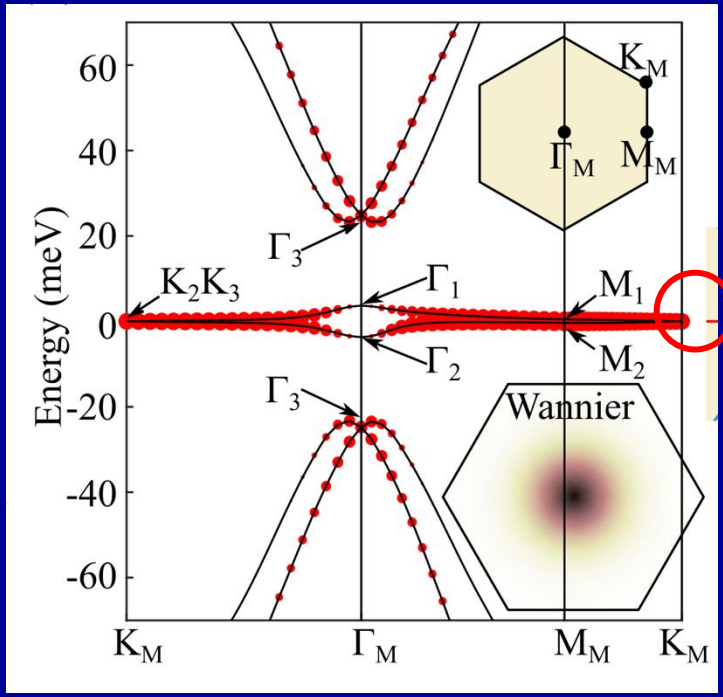

Band touching at K_M, $K_{M'}$
Protected by $C_{2z}T$
Total Chern: $C_1+C_2=0$
If broken: (e.g on hBN) C=-1,+1

	Graphene valley K	Graphene valley K'
Upper flat band	$C_+ = +1$	$C_+ = -1$
Lower flat band	$C_- = -1$	$C_- = +1$

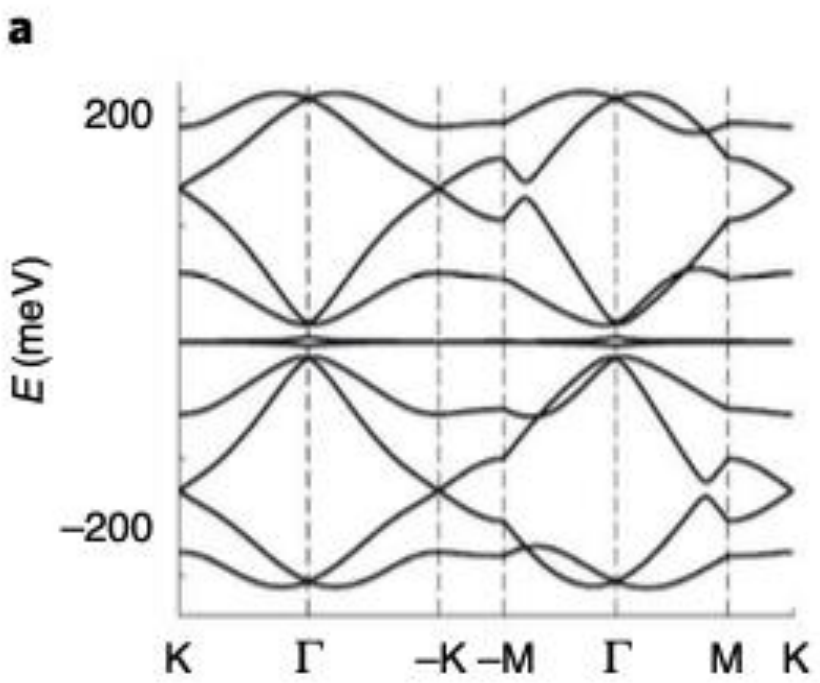

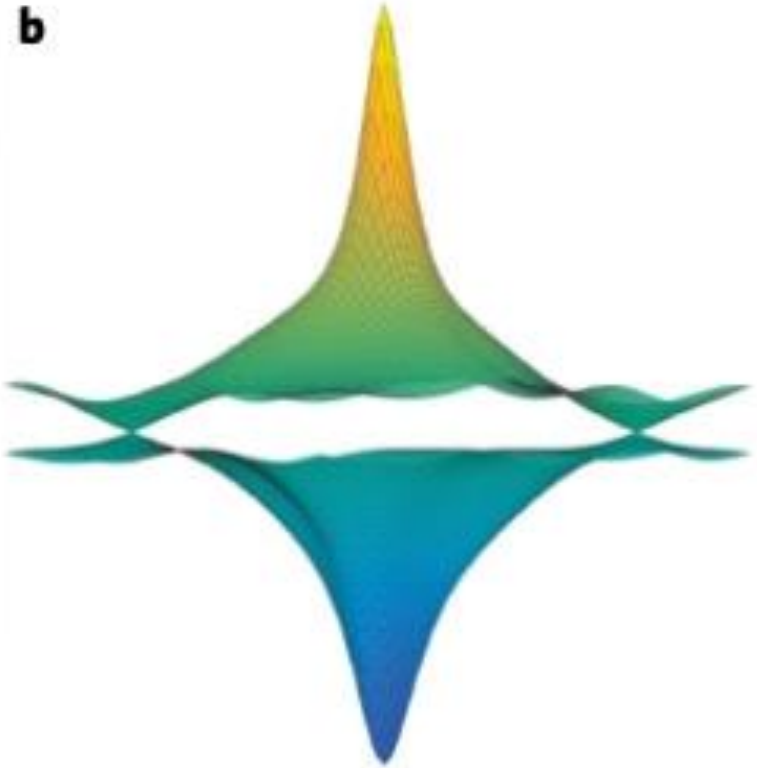

Fig. 6 | Moiré bands and Fermi surface. a, Moiré bands implied by a 10-band tight-binding model for the valley projected bands of MATBG. **b**, Energy versus momentum for the flat conduction and valence bands. Notice that the flat valence-band minimum is at Γ and that there are two linear band-touching Dirac points at the Brillouin-zone corners K and K′. These band models are constructed from electronic structure calculations performed at charge neutrality. Adapted with permission from: **a**, **b**, ref. [132], APS.

E.Andrei and A.MacDonald
Nature Mat. 19, 1265 (2020)

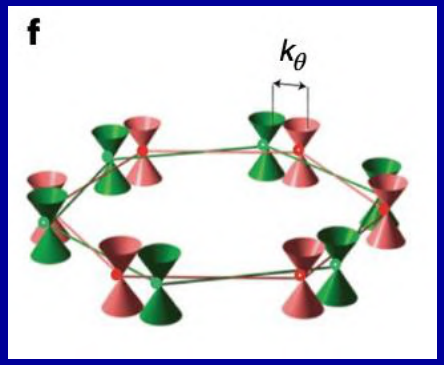

Band counting:

- The valleys at K and K' (of the original graphene layer) are decoupled
- The BM Hamiltonian for K (same for K') acts on 4-component spinors in (sublattice,layer) space: (A_1,B_1,A_2,B_2)
- This leads to 4 bands, BUT only 2 of them are close to E=0 forming the flat band manifold, the 2 others are at energies $\pm\hbar v_F|\Delta K|$
- Hence 2valleys/2 flat bands: 4 bands, accommodating 8 electrons max (counting spin)

Symmetries of the BM Model: Complete Table

Symmetry	Cond.	Type	Action on $H(\boldsymbol{k})$	$(\cdot)^2$
Moiré transl. $T_{\boldsymbol{L}_M}$	Always	Unit. spatial	$\boldsymbol{k} \in \mathrm{MBZ}$ is good quantum number; $H(\boldsymbol{k})$ block-diagonal.	$+1$
C_3	Always	Unit. spatial	$U_{C_3} H(R_{2\pi/3}\boldsymbol{k}) U_{C_3}^\dagger = H(\boldsymbol{k})$; $U_{C_3} = \mathrm{diag}(e^{i\pi/3}, e^{-i\pi/3}, e^{i\pi/3}, e^{-i\pi/3})$	$+1$
C_{2x} + layer swap	Always	Unit. spatial	$(\sigma_x \otimes \tau_x)\, H(-k_x, k_y)\, (\sigma_x \otimes \tau_x) = H(\boldsymbol{k})$; σ_x: $A \leftrightarrow B$; τ_x: layers $1 \leftrightarrow 2$	$+1$
$C_{2z}\mathcal{T}$ (single valley)	Always	Anti-unitary	$(\sigma_x \otimes \tau_0)\, H^*(\boldsymbol{k})\, (\sigma_x \otimes \tau_0) = H(\boldsymbol{k})$; $\boldsymbol{k} \to \boldsymbol{k}$; protects touching at K_M, K'_M	$+1$
Physical $\mathcal{T}$ (inter-valley)	Always	Anti-unitary	$K \leftrightarrow K'$, $\boldsymbol{k} \to -\boldsymbol{k}$; orbital repr.: $(\sigma_y \otimes \tau_y)\, H^*(-\boldsymbol{k})\, (\sigma_y \otimes \tau_y) = H(\boldsymbol{k})$; with spin: $\mathcal{T}^2 = -1$	-1
Valley $U(1)_v$	Always	Unit. internal	Valley $\xi = \pm$ conserved; no inter-valley scattering in $H(\boldsymbol{k})$	—
Spin $SU(2)_s$	Always	Unit. internal	$H(\boldsymbol{k})$ spin-independent; 2-fold spin degeneracy of every band	—
Chiral $\mathcal{C} = \sigma_z \otimes \tau_z$	$w_{AA} = 0$	Unit. internal	$\{\sigma_z \otimes \tau_z, H(\boldsymbol{k})\} = 0$; spectrum: $E \leftrightarrow -E$; flat bands pinned to $E = 0$	$+1$

Key remark

C_{2z} alone is **not** a symmetry at $\theta \neq 0$: it does not exchange layers, so the opposite sublattice winding $\boldsymbol{\sigma}^{(1)}$ vs $\boldsymbol{\sigma}^{(2)}$ is unaccounted for. Only $C_{2z}\mathcal{T}$ (mapping $\boldsymbol{k} \to \boldsymbol{k}$) is preserved.

Basis and notation

- Four-component spinor: $(A_1, B_1, A_2, B_2)^T$
- σ_μ: Pauli matrices in **sublattice** (A, B)
- τ_μ: Pauli matrices in **layer** $(1, 2)$
- $\tau_0 = \mathbb{1}_{2\times 2}$: layer identity

The quasi flat bands suggest that there may be a weakly broken Symmetry leading to exactly flat bands when restored…

Early STS evidence for flat bands

nature physics

LETTERS

PUBLISHED ONLINE: 29 NOVEMBER 2009 | DOI:10.1038/NPHYS1463

Observation of Van Hove singularities in twisted graphene layers

Guohong Li[1], A. Luican[1], J. M. B. Lopes dos Santos[2], A. H. Castro Neto[3], A. Reina[4], J. Kong[5] and E. Y. Andrei[1]*

Electronic instabilities at the crossing of the Fermi energy with a Van Hove singularity[1] in the density of states often lead to new phases of matter such as superconductivity[2,3], magnetism[4] or density waves[5]. However, in most materials this condition is difficult to control. In the case of single-layer graphene, the singularity is too far from the Fermi energy[6] and hence difficult to reach with standard doping and gating techniques[7]. Here we report the observation of low-energy Van Hove singularities in twisted graphene layers seen as two pronounced peaks in the density of states measured by scanning tunnelling spectroscopy. We demonstrate that a rotation between stacked graphene layers can generate Van Hove singularities, which can be brought arbitrarily close to the Fermi energy by varying the angle of rotation. This opens intriguing prospects for Van Hove singularity engineering of electronic phases.

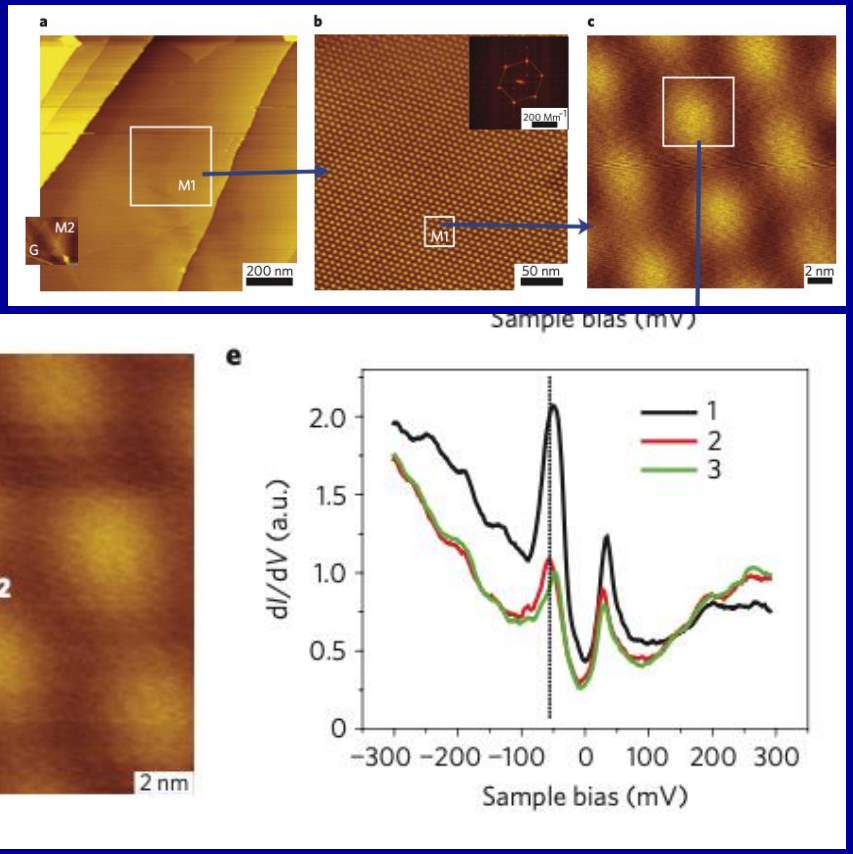

Why Flat Bands?
The Chiral Limit: connection with Landau Levels

TKV:

PHYSICAL REVIEW LETTERS **122,** 106405 (2019)

Editors' Suggestion

Origin of Magic Angles in Twisted Bilayer Graphene

Grigory Tarnopolsky, Alex Jura Kruchkov,* and Ashvin Vishwanath
Department of Physics, Harvard University, Cambridge, Massachusetts 02138, USA

w_{AA}=0 Extra symmetry
Particle-hole symmetric spectrum (E,-E)

Twisted bilayer graphene (TBG) was recently shown to host superconductivity when tuned to special "magic angles" at which isolated and relatively flat bands appear. However, until now the origin of the magic angles and their irregular pattern have remained a mystery. Here we report on a fundamental continuum model for TBG which features not just the vanishing of the Fermi velocity, but also the perfect flattening of the entire lowest band. When parametrized in terms of $\alpha \sim 1/\theta$, the magic angles recur with a remarkable periodicity of $\Delta\alpha \simeq 3/2$. We show analytically that the exactly flat band wave functions can be constructed from the doubly periodic functions composed of ratios of theta functions—reminiscent of quantum Hall wave functions on the torus. We further report on the unusual robustness of the experimentally relevant first magic angle, address its properties analytically, and discuss how lattice relaxation effects help justify our model parameters.

Remarkable connection to:

PHYSICAL REVIEW A VOLUME 19, NUMBER 6 JUNE 1979

Ground state of a spin-1/2 charged particle in a two-dimensional magnetic field

Y. Aharonov and A. Casher
Department of Physics and Astronomy, Tel Aviv University, Ramat Aviv, Israel
(Received 19 June 1978)

We prove that a spin-1/2 charged particle moving in a plane under the influence of a perpendicular magnetic field has $(N-1)$ zero-energy states, where N is the closest integer to the total flux in units of the flux quantum. The $(N-1)$ independent wave functions are calculated explicitly. The result, which is extremely simple to prove, is an example of the Atiyah-Singer index theorem when applied to the Euclidean two-dimensional Dirac equation.

See also:
Jie Wang et al.
PRR 3, 023155 (2021)

Prelude: the Aharonov-Casher theorem

Aharonov–Casher theorem (1979)

The number of normalisable zero modes of $D_{\mathbf{A}}$ in an arbitrary field $B(\boldsymbol{r})$ with total flux $\Phi = \int B\, d^2r$ is:

$$N_0 = \left\lfloor \frac{e\Phi}{2\pi} \right\rfloor = \left\lfloor \frac{\Phi}{\Phi_0} \right\rfloor, \qquad \Phi_0 = \frac{2\pi}{e} = \frac{2\pi\hbar}{e}. \tag{22}$$

Only the total flux matters; the spatial profile of $B(\boldsymbol{r})$ is irrelevant. The zero-mode wavefunctions are $f = e^{\phi} h(z)$ with $\nabla^2\phi = -B(\boldsymbol{r})$ and h holomorphic.

2D Dirac fermion in field $B(\boldsymbol{r})$

- $z = x + iy$; $\partial_z = \frac{1}{2}(\partial_x - i\partial_y)$
- $p_x - ip_y = -2i\partial_z$, $p_x + ip_y = -2i\partial_{\bar{z}}$
- Gauge field: $a_{\bar{z}} = \frac{e}{2}(A_x + iA_y)$, $a_z = a_{\bar{z}}^*$

- Zero modes **decouple**: $D_{\mathbf{A}} f = 0$ and $D_{\mathbf{A}}^\dagger g = 0$
- Ansatz: $f = e^{\phi(\boldsymbol{r})} h(z)$, $\partial_{\bar{z}} h = 0$
- $D_{\mathbf{A}} f = 0 \Rightarrow \partial_{\bar{z}}\phi = a_{\bar{z}}$ $\Rightarrow \nabla^2\phi = B(\boldsymbol{r})$

Zero-modes:

$\nabla^2\phi = B(\boldsymbol{r})$, $f = e^{\phi(\boldsymbol{r})} h(z)$

Uniform B: $\phi = -B|z|^2/4$

LLL: $f_n = e^{-B|z|^2/4} z^n$

Key contrast with TBLG

In AC, f and g **decouple**.
In TBLG they are **coupled** via αU
— the origin of magic angles.

Chiral Symmetry and the 2×2 Zero-Mode Operator

Chiral limit $w_{AA} = 0$

- $\{\sigma_z \otimes \tau_x, H\} = 0$: spectrum $E \leftrightarrow -E$, zero modes topologically protected
- $\sigma_z \otimes \tau_x$ splits the 4-spinor into two sectors: $C = +1$: (A_1, B_2) $\quad C = -1$: (B_1, A_2)
- Each sector: independent 2×2 problem

Index theorem and flat-band count

- $\mathcal{D}_\alpha$ is a twisted $\bar{\partial}$-operator on the moiré torus T^2
- Atiyah-Singer: $\mathrm{ind}(\mathcal{D}_\alpha) = 1$ per sector, for all α
- Riemann-Roch $\Rightarrow$ **2 flat bands** per spin-valley (1 per sector)
- These are *formal* zero modes;

2×2 operator (C

$U = \sum_{j=1}^{3} e^{i\mathbf{q}_j \cdot \mathbf{r}}, \quad \alpha = w/\hbar v_F K_D \theta$

$$\mathcal{D}_\alpha = \begin{pmatrix} D & \alpha U^* \\ \alpha U & -D^\dagger \end{pmatrix}, \quad \mathcal{D}_\alpha \begin{pmatrix} f \\ g \end{pmatrix} = 0$$

$$D = -2i\partial_z, \quad D^\dagger = -2i\partial_{\bar{z}}$$

Coupled equations

$$-2i\partial_{\bar{z}} f = -\alpha U^* g \qquad (1)$$

$$-2i\partial_z g = \alpha U f \qquad (2)$$

$f \in A_1, \quad g \in B_2$

TKV Ansatz: $f = e^{\phi} h(z)$ and the Poisson Equation

Step 1: scalar equation for f

- Apply $-2i\partial_z$ to (1); use (2)
- $D^\dagger D = -\nabla^2$ gives:

$$\left(-\nabla^2 + \alpha^2 |U|^2\right) f = 0$$

Step 2: ansatz $f = e^{\phi} h(z)$, ϕ real.

$\partial_{\bar{z}} h = 0$

- $\partial_{\bar{z}}(e^{\phi} h) = e^{\phi}(\partial_{\bar{z}}\phi) h$
- Substituting generates term $\propto (\partial_{\bar{z}}\phi)\partial_z h$
- Must set $\partial_{\bar{z}}\phi = 0$; ϕ real & periodic $\Rightarrow \phi = \text{const}$ (absorbed in norm.)

Step 3: solvability on $\mathbb{T}^2$

- $\int_{\text{cell}} \nabla^2 \phi \, d^2 r = 0 \Rightarrow$ source must have zero mean
- $\langle |U|^2 \rangle = 3 \Rightarrow$ subtract $B = 3\alpha^2$

Poisson equation for ϕ

$$\nabla^2 \phi = \alpha^2 |U(\boldsymbol{r})|^2 - 3\alpha^2$$

Unique real periodic solution $\forall\, \alpha$

$B = 3\alpha^2$: effective magnetic field

$e^{\phi} \longleftrightarrow e^{-\alpha B |z|^2/4}$ (LLL Gaussian)

Formal zero mode

$f = e^{\phi(r)} h(z)$, h holomorphic

h: theta function on $\mathbb{T}^2$
(section of degree-1 line bundle)

$\Rightarrow$ exists for **any** α;
normalisability of g is the extra condition

Common Zero of h and U: the Magic Angle Condition

g must be normalisable

- From (1): $g = \dfrac{2i(\partial_z\phi)e^{\phi}h}{\alpha U^*}$
- $U(\boldsymbol{r})$ has **one simple zero z_0/cell** (argument principle, winding number $= 1$)
- Near z_0: $U \approx c(z - z_0) \Rightarrow$ $g \propto 1/U^*$ diverges
- Regularity requires: $h(z_0) = 0$

One free parameter, one constraint

- h has **exactly one zero z_1/cell** (Abel's theorem, degree-1 bundle)
- Set $z_1 = z_0$: this fixes the zero of h
- Eq. (1) is now satisfied with regular g
- But eq. (2) is an **independent** constraint: $\alpha U f = -2i\partial_z g$

Magic angle condition

Plane-wave basis: $\mathcal{D}_\alpha \to \mathcal{M}(\alpha)$

$$\mathcal{F}(\alpha) = \det \mathcal{M}(\alpha) = 0$$

$\mathcal{F}$: entire in α^2, order 1
Hadamard $\Rightarrow$ infinite tower:

$$\mathcal{F}(\alpha) = \mathcal{F}(0)\prod_n \left(1 - \frac{\alpha^2}{(\alpha_n^*)^2}\right) e^{\alpha^2/(\alpha_n^*)^2}$$

Magic angles (TKV

$\alpha_1^* \approx 0.586$ $\quad \theta_1^* \approx 1.05°$
$\alpha_2^* \approx 2.221$ $\quad \theta_2^* \approx 0.28°$
$\alpha_3^* \approx 3.751$ $\quad \theta_3^* \approx 0.16°$

Spacing $\Delta\alpha \approx 1.6$; differ from full BM model ($w_{AA} = w_{AB}$)

QHE / Chiral-Limit Analogy (both on $\mathbb{T}^2$)

Concept	QHE on $\mathbb{T}^2$	TBLG chiral limit
Effective field	Uniform B (external)	$\alpha^2\lvert U\rvert^2$; mean $3\alpha^2$
Spinor coupling	Decoupled: $D_A f = 0$	Coupled: $Df = -\alpha U^* g$
Envelope eq.	$\nabla^2\phi = B$	$\nabla^2\phi = \alpha^2\lvert U\rvert^2 - 3\alpha^2$
Holomorphic h	Theta function	Theta function
Chern number	$N_\phi = \Phi/\Phi_0 \in \mathbb{Z}^+$	$C_1 = 1$ (topology)
Degeneracy	N_ϕ (Riemann-Roch)	2/spin-valley (Riemann-Roch)
Boundary cond.	Magnetic translations	Bloch quasi-periodicity
Extra cond.	None	$g = -Df/\alpha U^*$ regular
Special values	LLL $\forall\, N_\phi \in \mathbb{Z}^+$	Magic angles: $\mathcal{F}(\alpha_n^*) = 0$

The single key difference

On $\mathbb{T}^2$, both problems share the same structure: quasi-periodic e^{ϕ} times a theta function $h(z)$, degeneracy from Riemann-Roch. **Only difference:** in TBLG spinors are **coupled** via αU, requiring regularity of g, which generates magic angles.

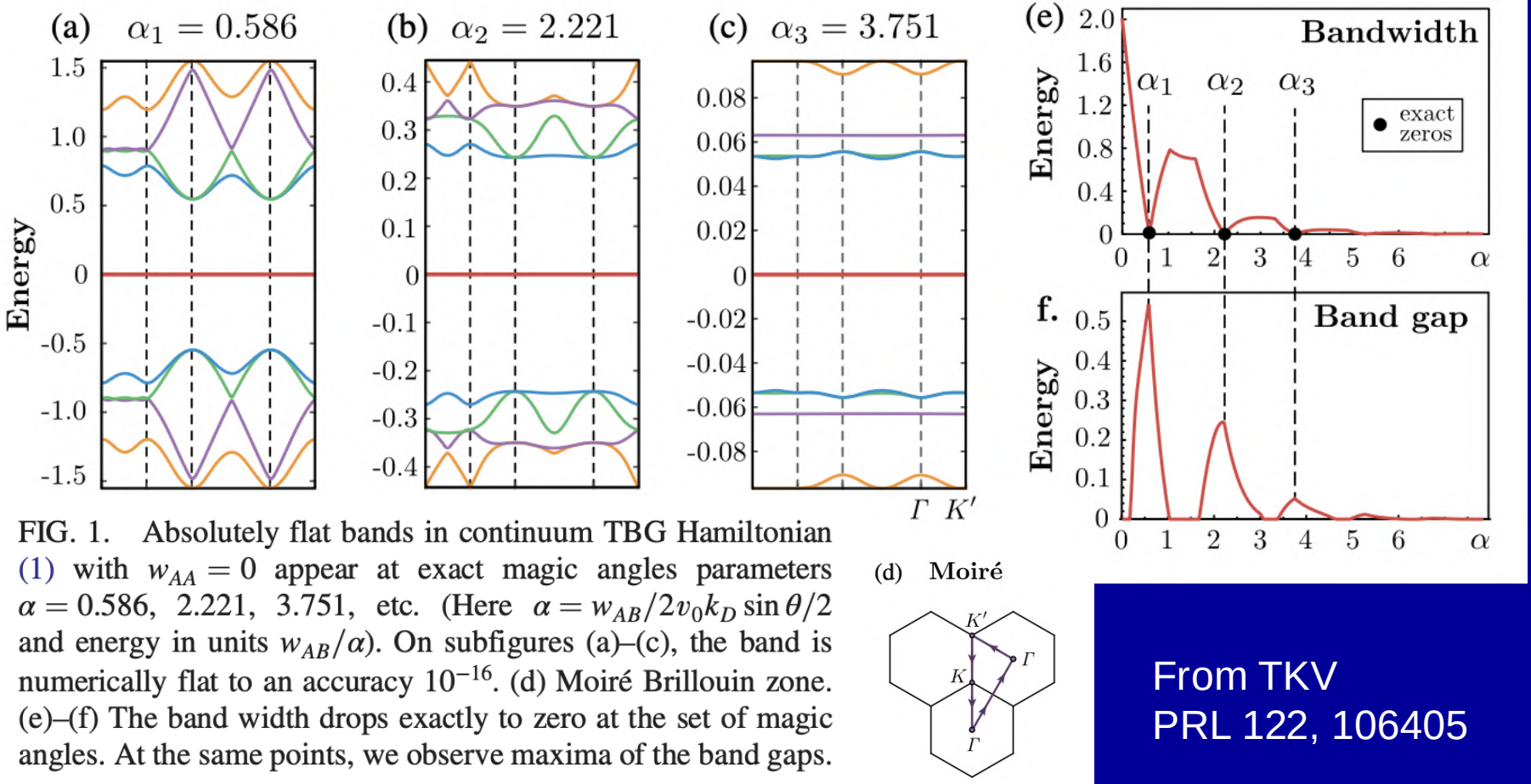

FIG. 1. Absolutely flat bands in continuum TBG Hamiltonian (1) with $w_{AA} = 0$ appear at exact magic angles parameters $\alpha = 0.586,\ 2.221,\ 3.751,$ etc. (Here $\alpha = w_{AB}/2v_0k_D \sin\theta/2$ and energy in units w_{AB}/α). On subfigures (a)–(c), the band is numerically flat to an accuracy 10^{-16}. (d) Moiré Brillouin zone. (e)–(f) The band width drops exactly to zero at the set of magic angles. At the same points, we observe maxima of the band gaps.

From TKV
PRL 122, 106405

TABLE I. Magic angles in models with $w_{AA} = 0$ and $w_{AA} = w_{AB}$. Only the principal magic angles α_1 coincide.

	α_1	α_2	α_3	α_4	α_5
$w_{AA} = 0$ (here)	0.586	2.221	3.75	5.28	6.80
$w_{AA} = w_{AB}$ ([29])	0.606	1.27	1.82	2.65	3.18

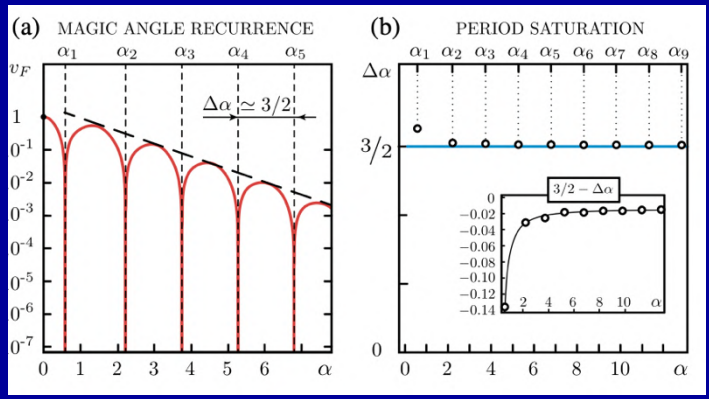

Wannier Model?

Band Topology and Wannier Obstruction

Topological character of flat bands

- Per spin-valley: Chern number $C = \pm 1$
- Flat-band pair: $\mathbb{Z}_2$ **fragile topological invariant** [Po et al. 2018; Ahn et al. 2019]
- C_3-symmetric **Wannier obstruction**: no symmetric exponentially localized Wannier functions for the flat bands alone

Implications

- Any real-space model must include remote bands or resolve the obstruction by other means
- Berry phase π around K_M: Dirac fermion character persists
- THF model resolves this via topological c-electrons

Symmetry group

$$\{C_3,\ C_{2x},\ \mathcal{T}\} \Rightarrow \text{wallpaper group } p\bar{6}m2$$

Flat-band topology

Per spin-valley flavor:

$$C = \pm 1, \qquad \text{fragile } \mathbb{Z}_2$$

Total: $4 \times 2 = 8$ electrons/moiré cell

Key tension

STM $\Rightarrow$ charge localized at AA sites

Topology $\Rightarrow$ no symmetric Wannier functions!

Resolved by the **heavy fermion model**.

“Fragile” Topology

PHYSICAL REVIEW LETTERS **121,** 126402 (2018)

Editors' Suggestion

Fragile Topology and Wannier Obstructions

Hoi Chun Po,[1] Haruki Watanabe,[2] and Ashvin Vishwanath[1]
[1]*Department of Physics, Harvard University, Cambridge, Massachusetts 02138, USA*
[2]*Department of Applied Physics, University of Tokyo, Tokyo 113-8656, Japan*

Application to TBLG:

PHYSICAL REVIEW B **99,** 195455 (2019)

Editors' Suggestion

Faithful tight-binding models and fragile topology of magic-angle bilayer graphene

Hoi Chun Po,[1,2] Liujun Zou,[1,2] T. Senthil,[2] and Ashvin Vishwanath[1]
[1]*Department of Physics, Harvard University, Cambridge, Massachusetts 02138, USA*
[2]*Department of Physics, Massachusetts Institute of Technology, Cambridge, Massachusetts 02139, USA*

Multi-band models (up to 10)

The Song-Bernevig `Topological Heavy-Fermion' Model

PRL 129, 047601 (2022)

Several other Wannier constructions see e.g. Carr et al. PRR 1, 033072 (2019)

- Introduce two types of orbitals:
- Localized "f" orbitals centered on AA stacking regions
- (In agreement w/ STM, this will carry most of the charge)
- Conduction "c" orbitals carrying the topology

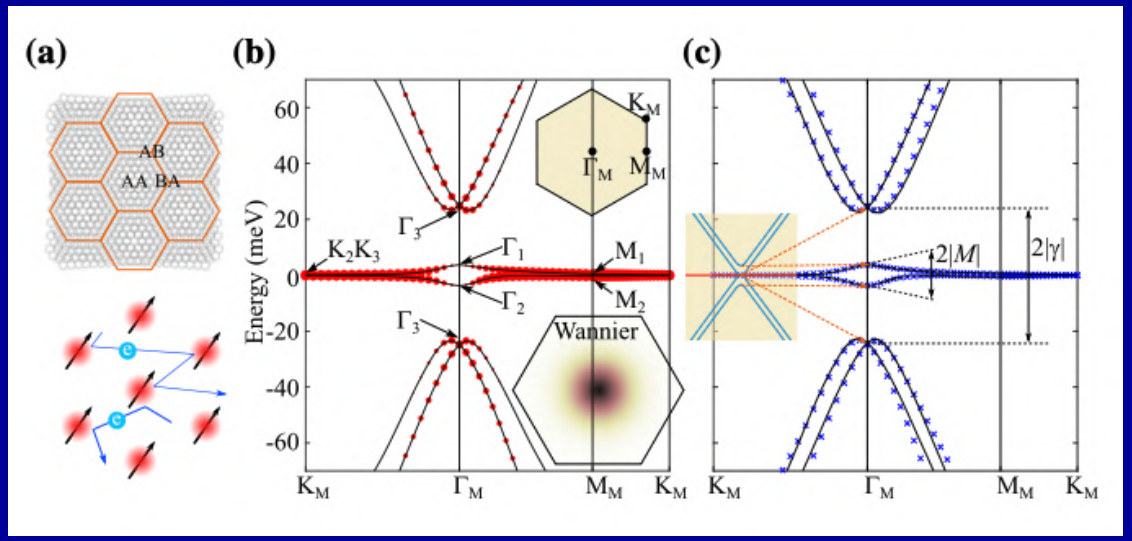

FIG. 1. Topological heavy fermion model. (a) A sketch of the moiré unit cell of MATBG and its heavy fermion analog, where the local moments and itinerant electrons are formed by the effective f orbitals at the AA-stacking regions and topological conduction bands (c), respectively. (b) The band structure of the

The 2 flat bands have mostly f-character, except near Gamma

conduction bands (c), respectively. (b) The band structure of the BM model at the magic angle $\theta = 1.05°$, where the moiré BZ and high symmetry momenta are illustrated in the upper inset panel. The overlaps between the Bloch states and the trial WFs are represented by the red circles. The density profile of the constructed maximally localized WFs (f orbitals) is shown in the lower inset panel. (c) Bands given by the topological heavy fermion model (black lines) compared to the BM bands (blue crosses). The c (blue) and f bands (red) in the decoupled limit, where $\gamma = v'_\star = 0$, are shown in the inset. Orange dashed lines indicate the evolution of energy levels as f-c coupling is turned on.

The THF Model: f- and c-Electrons

f-orbitals (local moments)

- Localized at AA sites (triangular lattice, spacing L_M)
- $p_x \pm ip_y$ orbital symmetry (consistent with C_3, $C_{2z}\mathcal{T}$)
- Quantum numbers: spin s, valley η, orbital $\alpha = \pm$
- 8-fold degenerate per moiré unit cell
- Dispersionless at $\epsilon_f \approx 0$

c-electrons (topological conduction bath)

- Extended Dirac cones at K_M, K'_M in MBZ
- Chern number $C = \pm 1$ per spin-valley flavor
- Mass gap M: symmetry-allowed, topologically essential
- Renormalized velocity $v_c \approx 0.4\, v_F$
- Bandwidth $\sim \hbar v_c K_D \theta \sim \gamma$

f-electron term

$$H_f = \epsilon_f \sum_{\boldsymbol{R},\alpha,s,\eta} f^\dagger_{\boldsymbol{R}\alpha s\eta} f_{\boldsymbol{R}\alpha s\eta}$$

c-electron term

$$h_c(\boldsymbol{k}) \approx \hbar v_c \boldsymbol{\sigma} \cdot \boldsymbol{k} + M\sigma_z$$

Two Dirac cones with mass $M \approx 3.7\,\text{meV}$

THF parameters at magic angle

$\epsilon_f \approx 0$, $M \approx 3.7\,\text{meV}$, $\gamma \approx 24.8\,\text{meV}$, $v_c \approx 0.4\, v_F$

f-c hybridization

$$H_{fc} = \frac{1}{\sqrt{N}} \sum_{\boldsymbol{R},\boldsymbol{k},\alpha,\eta,s} \gamma_{\alpha\eta}(\boldsymbol{k})\, f^\dagger_{\boldsymbol{R}\alpha s\eta} c_{\boldsymbol{k}\eta s} e^{i\boldsymbol{k}\cdot\boldsymbol{R}} + \text{h.c.}$$

Coulomb interaction: screening by gates

- What is the screened Coulomb interaction?
- How is TBG actually realized experimentally? Does this affect the interaction strength?

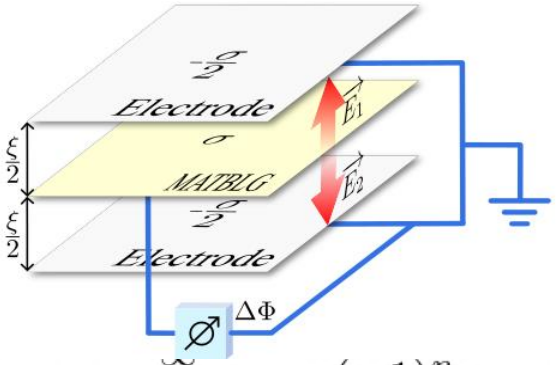

- Double-gate screened Coulomb potential → dependence on gate distance
- Two-body overlap integrals
- Local and non-local interaction terms

$$V(\mathbf{r}) = U_\xi \sum_{n=-\infty}^{\infty} \frac{(-1)^n}{\sqrt{(\mathbf{r}/\xi)^2 + n^2}}$$

$$\hat{H}_I = \frac{1}{2}\int d^2\mathbf{r}_1 d^2\mathbf{r}_2 V(\mathbf{r}_1 - \mathbf{r}_2) : \hat{\rho}(\mathbf{r}_1) :: \hat{\rho}(\mathbf{r}_2) :$$

$$\hat{H}_I = \hat{H}_{U_1} + \hat{H}_W + \hat{H}_V + \hat{H}_J$$

Z.D. Song, B.A. Bernevig (PRL 2022)

f-f density-density
U_1: on-site (~60 meV)
$\propto \hat{n}^f_s \hat{n}^f_{s'}$

c-f density-density
(~50 meV)
$\propto \hat{n}^f_s \hat{n}^c_{s'}$

c-c density-density
(~50 meV)
$\propto \hat{n}^c_s \hat{n}^c_{s'}$

c-f exchange (~16 meV)
$\propto f^\dagger_s f_{s'} c^\dagger_{s'} c_s$

It is very natural to deal with interactions in this model using Dynamical Mean-Field Theory

Rai et al. PRX 14, 031045 (2024); Crippa et al. arXiv:2509.19436

Related work: M.Calderon, E.Bascones et al. Nat Comm 2023, PRB 2025

Phys. Rev. Lett. **131**, 166501 (2023) | Phys. Rev. X **14**, 031045 (2024) | Nature **650**, 592–598 (2026) | arXiv:2509.19436

Compressibility measurements

Article

Cascade of phase transitions and Dirac revivals in magic-angle graphene

https://doi.org/10.1038/s41586-020-2373-y
Received: 25 November 2019

U. Zondiner[1,5], A. Rozen[1,5], D. Rodan-Legrain[2,5], Y. Cao[2], R. Queiroz[1], T. Taniguchi[3], K. Watanabe[3], Y. Oreg[1], F. von Oppen[4], Ady Stern[1], E. Berg[1], P. Jarillo-Herrero[2]✉ & S. Ilani[1]✉

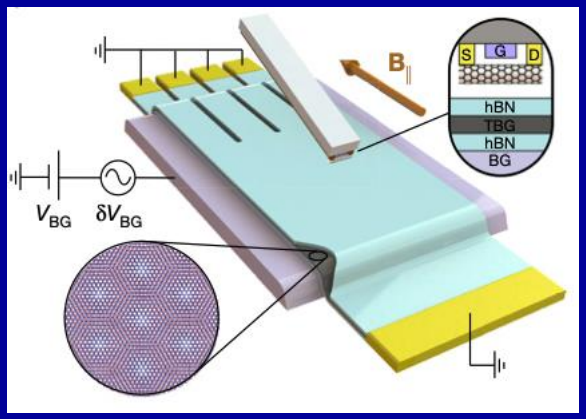

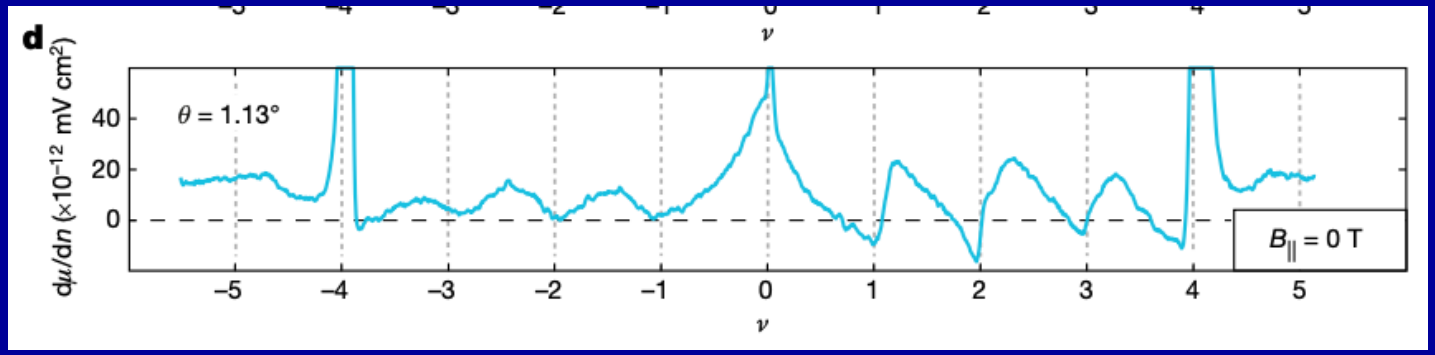

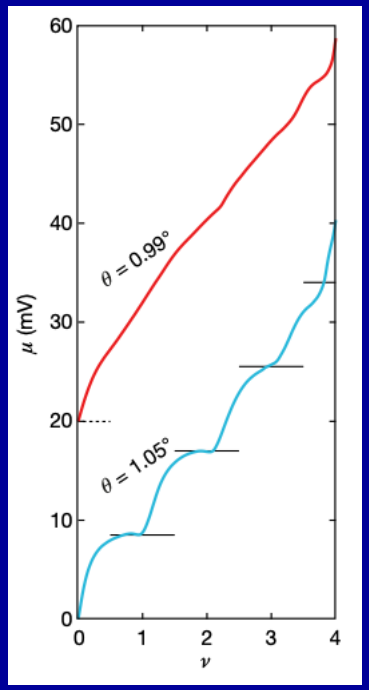

Electronic compressibility: $\kappa = \frac{\partial \nu}{\partial \mu}$

Einstein relation:
conductivity=diffusivity*compressibility $\sigma = \kappa D$

Article

Flavour Hund's coupling, Chern gaps and charge diffusivity in moiré graphene

https://doi.org/10.1038/s41586-021-03366-w
Received: 26 August 2020

Jeong Min Park[1,4], Yuan Cao[1,4]✉, Kenji Watanabe[2], Takashi Taniguchi[3] & Pablo Jarillo-Herrero[1]✉

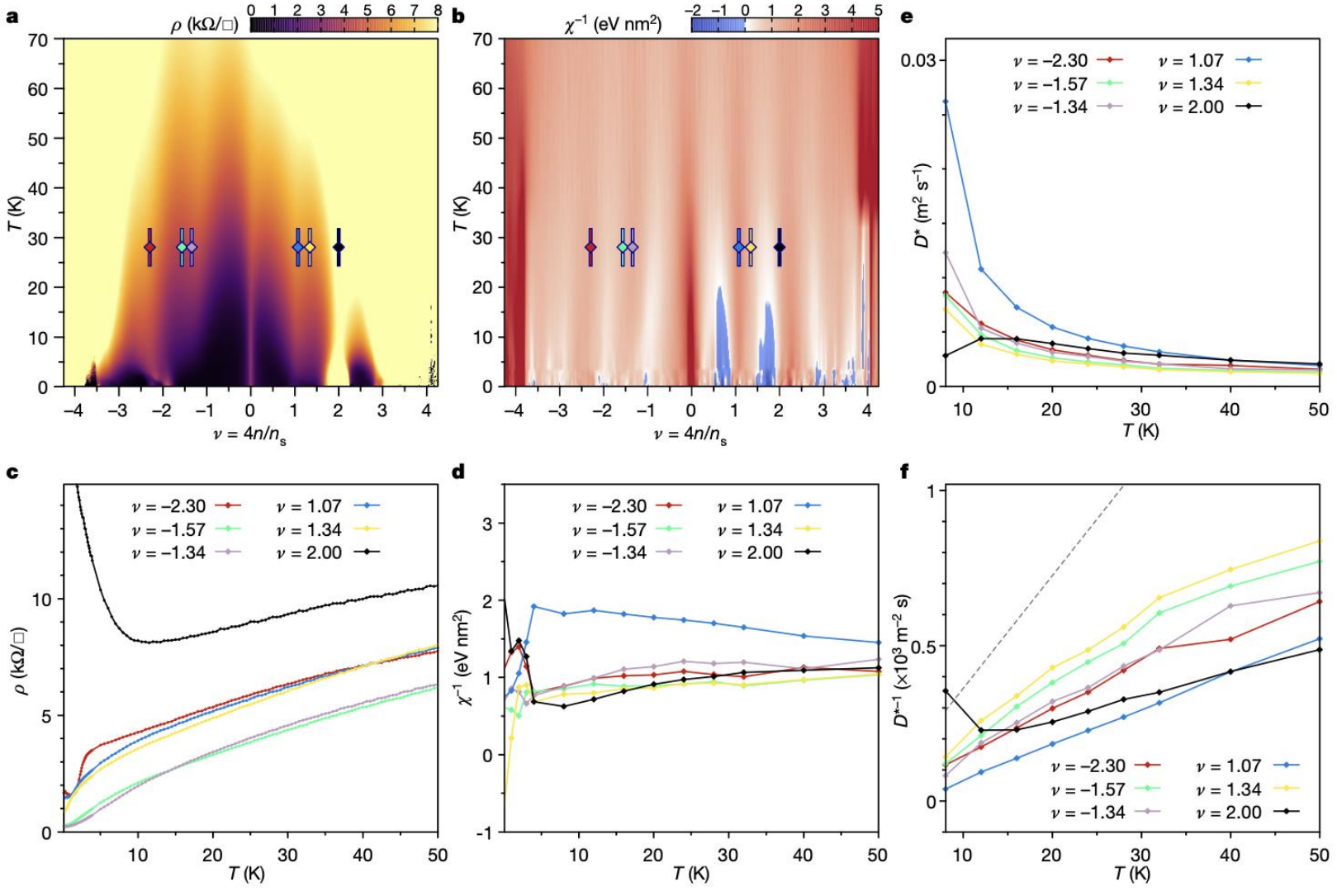

Compressibility from DMFT

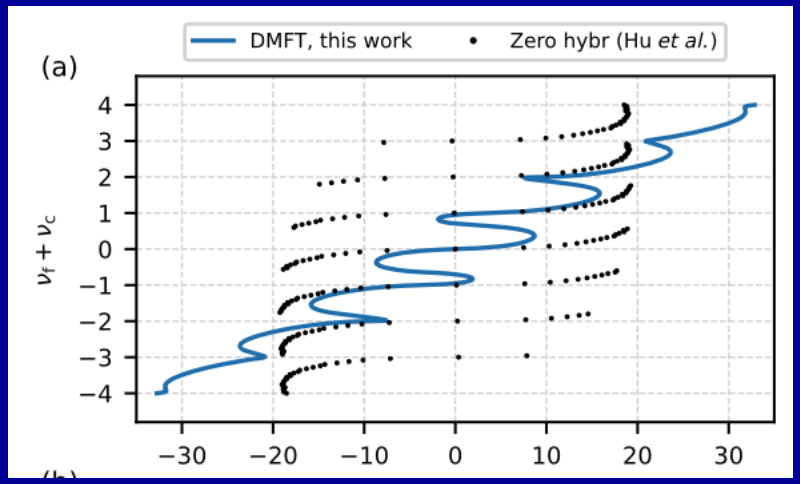

$\nu_f + \nu_c$ vs. μ

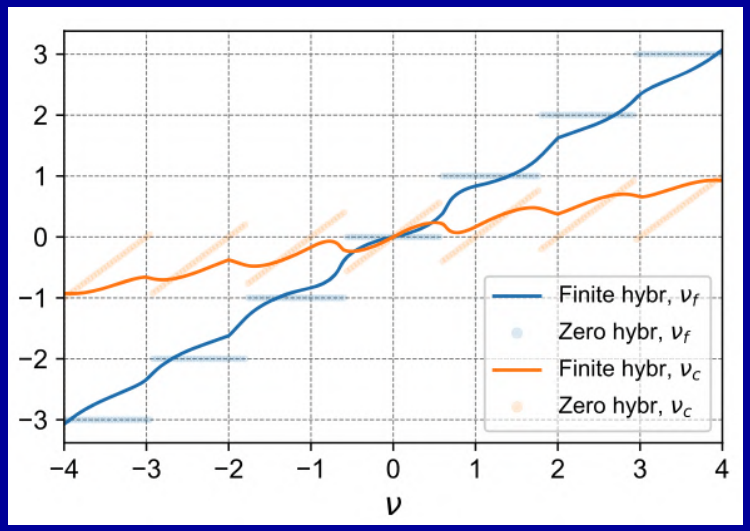

ν_f , ν_c vs. ν

Without strain and relaxation
G.Rai et al. PRX 14, 031045 (2024):

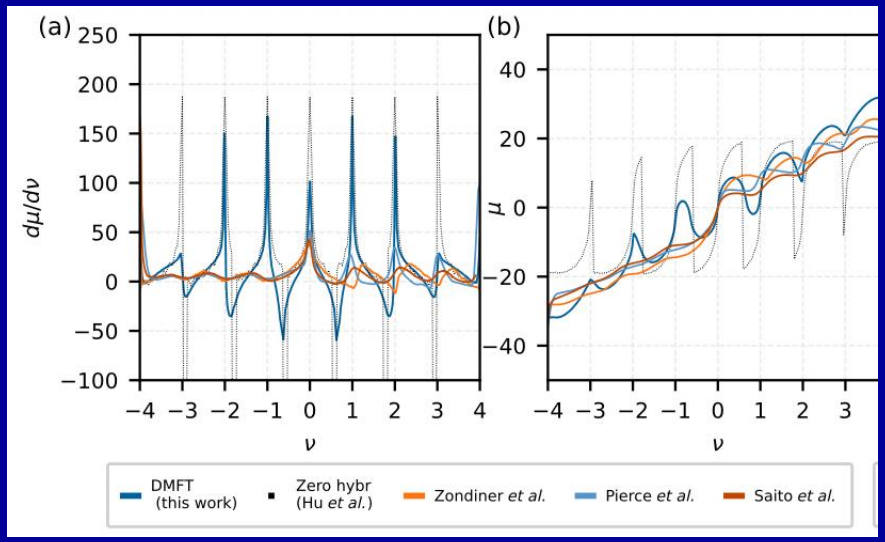

With strain and relaxation
L.Crippa et al arXiv:2509.19436:

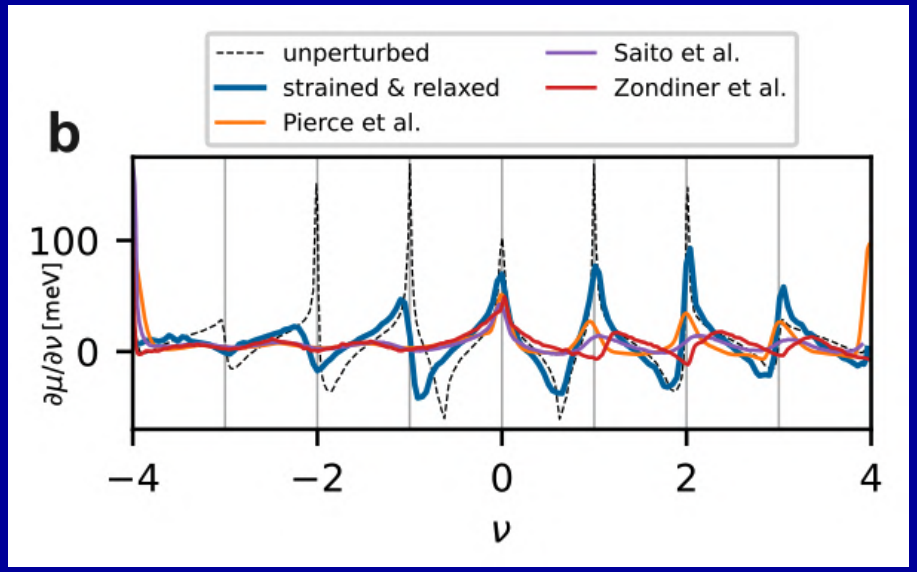

Entropy and Pomeranchuk Effect

Article

Isospin Pomeranchuk effect in twisted bilayer graphene

https://doi.org/10.1038/s41586-021-03409-2

Received: 25 August 2020

Yu Saito[1,2,7], Fangyuan Yang[1,7], Jingyuan Ge[1], Xiaoxue Liu[3], Takashi Taniguchi[4], Kenji Watanabe[5], J. I. A. Li[3], Erez Berg[6] & Andrea F. Young[1]✉

Article

Entropic evidence for a Pomeranchuk effect in magic-angle graphene

https://doi.org/10.1038/s41586-021-03319-3

Received: 4 September 2020

Accepted: 29 January 2021

Asaf Rozen[1,4], Jeong Min Park[2,4], Uri Zondiner[1,4], Yuan Cao[2,4], Daniel Rodan-Legrain[2], Takashi Taniguchi[3], Kenji Watanabe[3], Yuval Oreg[1], Ady Stern[1], Erez Berg[1]✉, Pablo Jarillo-Herrero[2]✉ & Shahal Ilani[1]✉

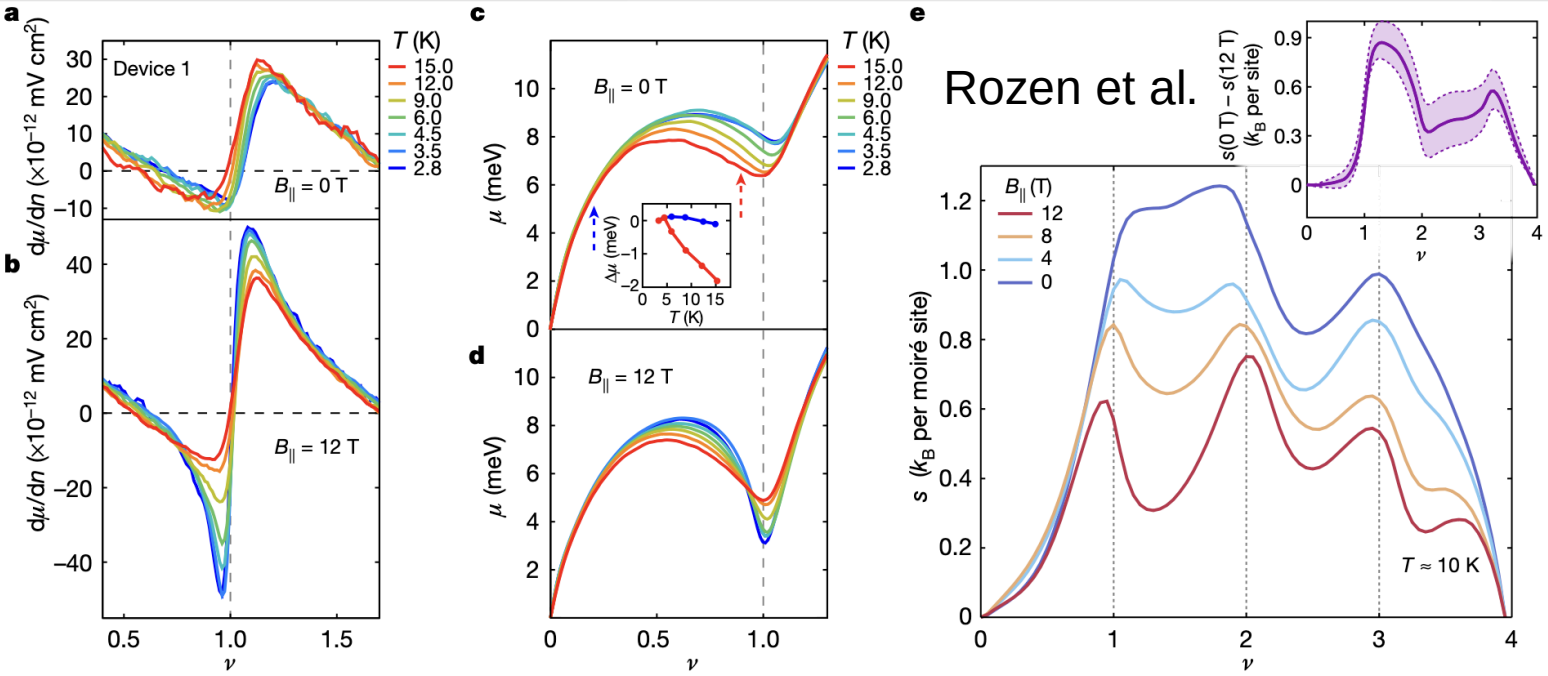

Fig. 2 | Measurement of large magnetic entropy above $\nu = 1$. a, Inverse compressibility, $d\mu/dn$, as a function of ν, near $\nu = 1$, measured at zero parallel magnetic field, $B_{\parallel} = 0$ T, and at several temperatures (see key). With increasing T, the jump in $d\mu/dn$ moves towards lower ν and becomes stronger. **b**, Same measurement as **a** but done at $B_{\parallel} = 12$ T. Here, opposite to the zero-field case, increasing T reduces the magnitude of the $d\mu/dn$ jump, as expected from thermal smearing. **c**, The chemical potential μ (relative to that of the charge neutrality point) versus ν at $B_{\parallel} = 0$ T, obtained by integrating the $d\mu/dn$ signal in **a** with respect to n. Inset, $\Delta\mu$ (defined as $\mu(T,\nu) - \mu(T = 2.8\,\mathrm{K}, \nu)$) as a function of temperature for $\nu = 0.2$ (blue) and $\nu = 0.9$ (red). At $\nu = 0.2$ the chemical potential is nearly temperature independent, whereas at $\nu = 0.9$ it is roughly constant until $T \approx 4$ K and then starts decreasing approximately linearly with T. **d**, Similar to **c** but at $B_{\parallel} = 12$ T. In contrast to the zero-field case, here, below $\nu \approx 0.9$, μ decreases with T while above $\nu \approx 0.9$, μ increases with T. **e**. The electronic entropy s (in units of k_B per moiré unit cell) as a function of ν at $T \approx 10$ K and at various parallel magnetic fields, $B_{\parallel} = 0, 4, 8, 12$ T (see key). To obtain the entropy we determine the partial derivative $(\partial\mu/\partial T)_{\nu,B_{\parallel}}$ from a linear fit to the measured μ versus T in the range $T = 4.5$–15 K. The entropy per moiré cell is then obtained by integrating Maxwell's relation, $(\partial s/\partial \nu)_{T,B_{\parallel}} = -(\partial\mu/\partial T)_{\nu,B_{\parallel}}$, over ν (see Supplementary Information for details). At $B_{\parallel} = 0$, the entropy climbs rapidly near $\nu = 1$ to a value of about $1.2 k_B$ per moiré cell. Inset, the difference between the entropies at low and high fields, $s(B_{\parallel} = 0\,\mathrm{T}) - s(B_{\parallel} = 12\,\mathrm{T})$. The purple shading shows the estimated standard deviation due to the measurement accuracy.

$$\frac{\partial S}{\partial \nu}\Big|_T = -\frac{\partial \mu}{\partial T}\Big|_\nu$$

cf. last year's lectures

magnetic field. This reveals a phase diagram that is consistent with a Pomeranchuk-like temperature- and field-driven transition from a low-entropy electronic liquid to a high-entropy correlated state with nearly free magnetic moments. The correlated state features an unusual combination of seemingly contradictory properties, some associated with itinerant electrons—such as the absence of a thermodynamic gap, metallicity and a Dirac-like compressibility—and others associated with localized moments, such as a large entropy and its disappearance under a magnetic field. Moreover, the energy scales characterizing

Note: the electronic Pomeranchuk effect was first predicted by DMFT in the context of the Hubbard model…

PHYSICAL REVIEW B VOLUME 48, NUMBER 10 1 SEPTEMBER 1993-II

Physical properties of the half-filled Hubbard model in infinite dimensions

Antoine Georges*
Laboratoire de Physique Théorique de l'Ecole Normale Supérieure, 24, rue Lhomond, 75231 Paris Cedex 05, France
Werner Krauth†

$$\frac{\partial s}{\partial U} = -\frac{\partial d}{\partial T}.$$

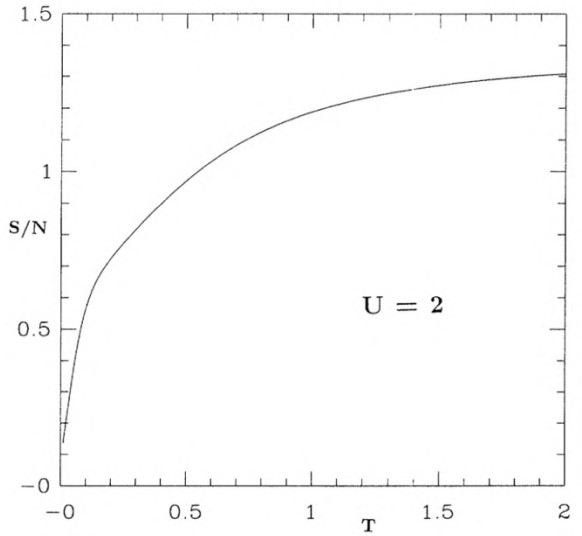

FIG. 5. Entropy per lattice site S/N vs temperature for $U=2$ (hc lattice). The value ln2 is reached roughly at the spin fluctuation scale T_F^*.

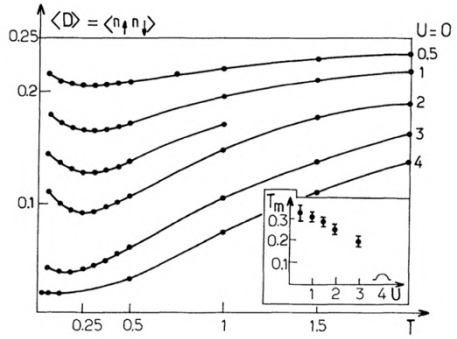

FIG. 6. Fraction of doubly occupied sites $\langle D \rangle$ vs temperature for the hc lattice with $U=0$, 0.5, 1, 2, 3, 4 (exact enumeration and Monte Carlo results). Inset: Temperature T_m at which the minimum of $\langle D \rangle$ vs T is found, as a function of U. For $U=4$, we cannot find a minimum down to the lowest temperature studied ($\beta=32$).

PRL 95, 056401 (2005) PHYSICAL REVIEW LETTERS week ending 29 JULY 2005

Interaction-Induced Adiabatic Cooling and Antiferromagnetism of Cold Fermions in Optical Lattices

F. Werner,[1,2] O. Parcollet,[3] A. Georges,[2] and S. R. Hassan[2]

Pomeranchuk effect:

- Coherent quasiparticles at low-T (T-linear entropy, Fermi liquid regime)
- Get partially converted into local moments as they loose coherence upon heating
- While still displaying metallic-like transport

PRL 110, 086401 (2013) PHYSICAL REVIEW LETTERS week ending 22 FEBRUARY 2013

How Bad Metals Turn Good: Spectroscopic Signatures of Resilient Quasiparticles

Xiaoyu Deng,[1,2,3] Jernej Mravlje,[4,1,5] Rok Žitko,[5] Michel Ferrero,[1] Gabriel Kotliar,[3] and Antoine Georges[4,1,6,2]

arXiv:2601.09420

Quasiparticle to local moment crossover in bad metals

A. Chen,[1,*] F. B. Kugler,[2,3,*] P. Doležal,[1,4] Y. Saito,[5,6] A. Kawamoto,[5] A. Georges,[7,3,8,9] and A. Pustogow[1,†]

TBLG Entropy

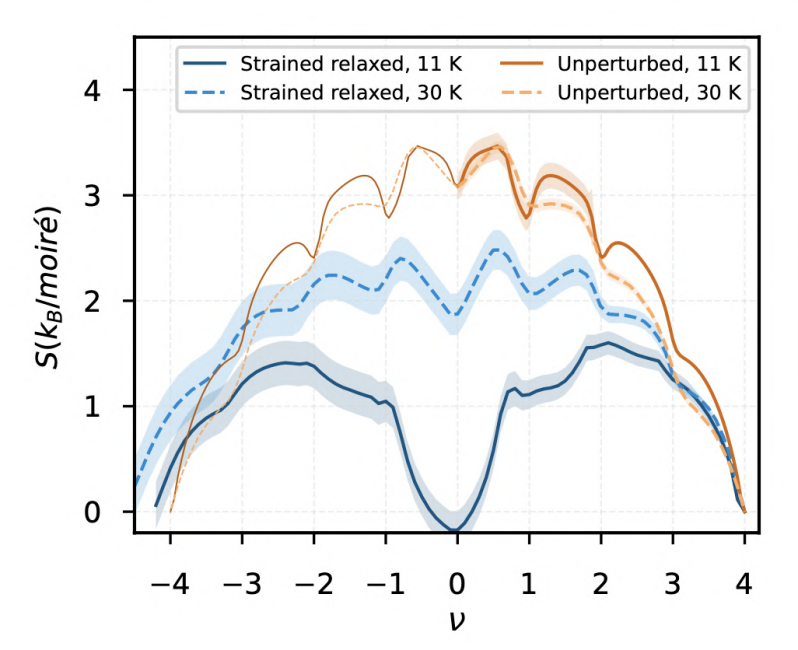

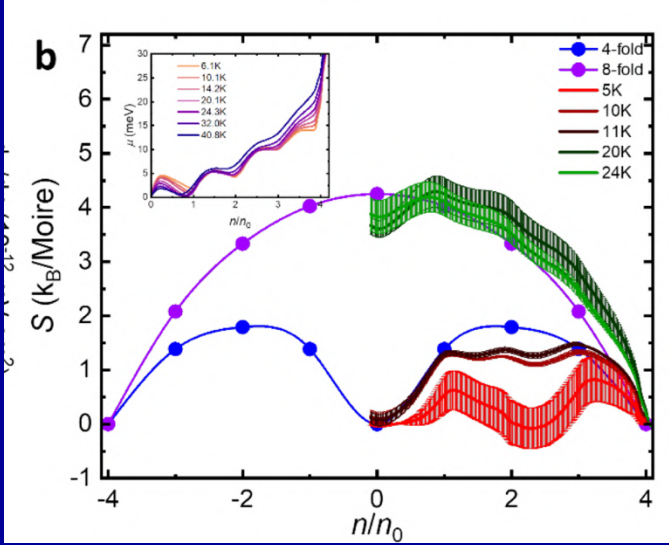

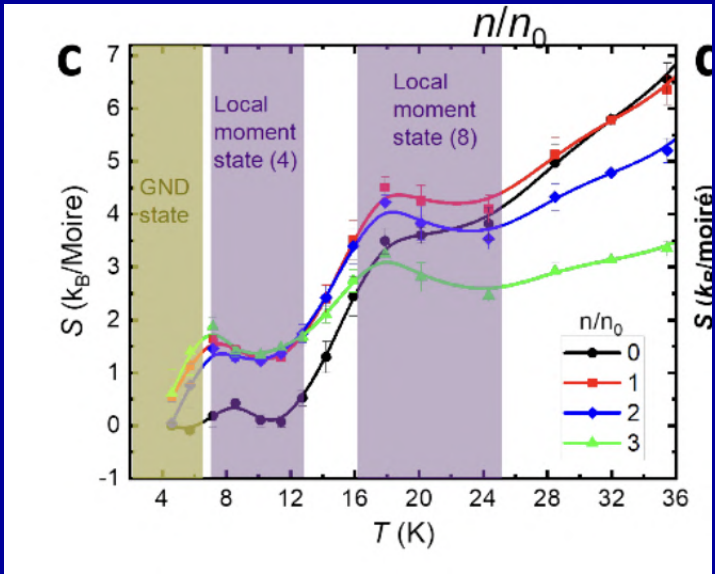

Theory – THF model+DMFT (Crippa et al arXiv:2509.19436)

Experiments (E.Andrei's group) Zhang et al. arXiv:2503.17875

TBLG: Some Open Questions (Among many)

- Origin of Strange Metal (~ T-linear resistivity) behaviour?
- Mechanism for superconductivity?
- Symmetry of the SC order parameter?
- Many more…